ARTICLE IN PRESS

Quaternary International xxx (xxxx) xxx

Contents lists available at ScienceDirect

Quaternary International

journal homepage: www.elsevier.com/locate/quaint

Late Holocene evolution of a Mediterranean incised river flowing to the Atlantic: Sedimentary dynamics, fluvial activity and paleoenvironmental reconstruction (SW Iberia)

Ana Maria Costa [a,b,c,*], Maria da Conceição Freitas [c,d], Manel Leira [c,e,f], Rita Fonseca [g,h], João Duarte [i], Mariana Diniz [j], Pablo Arias [b]

[a] LARC – DGPC and CIBIO / InBIO, Calçada do Mirante à Ajuda, n° 10A, 1300-418, Lisboa, Portugal
[b] IIIPC (Universidade de Cantábria, Gobierno de Cantabria), Avda de los Castros 52, 39005, Santander, Spain
[c] Instituto Dom Luiz (IDL), Faculdade de Ciências, Universidade de Lisboa, Edifício C6, Piso 3, Campo Grande, 1749-016, Lisboa, Portugal
[d] Departamento de Geologia, Faculdade de Ciências, Universidade de Lisboa, Edifício C6, Piso 3, Campo Grande, 1749-016, Lisboa, Portugal
[e] BioCost Research Group, Facultade de Ciencias and Centro de Investigacións Científicas Avanzadas (CICA), Universidade de A Coruña, 15071, A Coruña, Spain
[f] Biodiversity and Applied Botany Research Group, Departmento de Botánica, Facultade de Bioloxía, Universidade de Santiago de Compostela, 15782, Santiago de Compostela, Spain
[g] Departamento de Geociências, Instituto de Ciências da Terra (ICT), Universidade de Évora, Rua Romão Ramalho 59, 7002-554, Évora, Portugal
[h] Laboratório de Biogeoquímica Ambiental, Universidade de Évora, Colégio Pedro da Fonseca, Parque Industrial e Tecnológico, Rua da Barba Rala n° 1, 7005-345, Évora, Portugal
[i] Instituto Hidrográfico, Rua das Trinas 49, 1296-093, Lisboa, Portugal
[j] UNIARQ, Universidade de Lisboa, Alameda da Universidade, 1600-214, Lisboa, Portugal

ARTICLE INFO

Keywords:
Mediterranean estuaries
Sedimentation rates
Sensitive-environmental proxies
High-resolution proxy analyses
Chronology
Sado river

ABSTRACT

The aims of this work are to characterize the paleoenvironmental evolution and the sedimentary fluvial responses to climate and river flow changes of the upstream reaches of the Sado estuary since the Mid-Late Holocene. By combining the previous information, we also intent to define the limit of the fluvial-estuarine boundary and maximum limit of tidal influence of the estuarine area during the last 4500 years.

To accomplish these objectives a 10.5 m-long sediment core was collected at ca. 65 km upstream the Sado estuary inlet and studied using multiproxy analyses and radiocarbon dating. In addition, multi-proxy data from sediment cores and superficial samples collected downstream, in the alluvial plain and intertidal areas near the present-day fluvial-estuarine boundary, were combined and contributed to the interpretations. We concluded that: i) the organic matter is mostly sourced in terrestrial/freshwater environments even during periods with marine influence, as suggested by the occurrence of marine benthic diatoms between 4300 and 4200 cal BP; ii) the fluvial-estuarine boundary retreat during the Middle to Late Holocene transition (4350-4000 cal BP) reaching areas of the Sado river (Laxique), located ca. 15 km upstream of the present-day boundary; iii) modifications on the location of the fluvial-estuarine boundary are mostly derived from drier climatic conditions and consequent flow river discharges; iv) the aggradation and progradation of the alluvial plain started at ca. 4000 cal BP at Laxique (and at ca. 3240 cal BP at Arapouco); and v) the abrupt change in the sedimentation rates and sedimentation pattern before and after the beginning of the alluvial plain aggradation process (4000 cal BP at Laxique and 3240 cal BP at Arapouco) reflects essentially changes in the fluvial activity and the loss of accomodation space.

1. Introduction

Mediterranean rivers are characterized by irregular flows (e.g. Oueslati et al., 2015) that are mostly dependent on climate prevailing conditions (e.g. Thornes et al., 2009). Rivers can experience extreme floods during prevalent continental wet conditions or become intermittent due to the occurrence of severe droughts (e.g. Thornes et al., 2009; Cid et al., 2017). In the Mediterranean area, river flows are

* Corresponding author. LARC – DGPC and CIBIO / InBIO, Calçada do Mirante à Ajuda, n° 10A, 1300-418, Lisboa, Portugal.
E-mail address: acosta@dgpc.pt (A.M. Costa).

https://doi.org/10.1016/j.quaint.2021.12.002
Received 21 August 2021; Received in revised form 30 November 2021; Accepted 1 December 2021
Available online 4 December 2021
1040-6182/

strongly influenced by seasonal precipitation variability, with maximum discharges occurring during the autumn and winter, and minimum flows occurring during the summer (e.g. Thornes et al., 2009; Benito et al., 2015). South Iberia, following the climatic conditions of western Mediterranean areas, presents rainfall seasonality during autumn and winter (Benito et al., 2015), and is nowadays characterized by large inter-annual variability of precipitation and consequently river flows vary by large disparities between wet and dry years (e.g. Trigo et al., 2004).

At present, the hydrological pattern of rivers is measured by instrumental data, being the natural flow regime of several rivers significantly altered by the construction of dams over the last decades. Notwithstanding, in the past, river flow regimes and sedimentary and environmental changes can only be achieved from the information retained in the sedimentary record, preserved both in their organic and inorganic components. The sedimentary infilling of coastal incised valleys is, then, a key that allows to reconstruct the evolution of an area, the occurrence of extreme events, the role of local environmental factors in the sedimentation patterns, particularly after the deceleration of the sea level rise (that for the Portuguese coast was estimated to occur ca. 7000 cal BP; Vis et al., 2008; Leorri et al., 2012; García-Artola et al., 2018), and the anthropic influence in more recent times (e.g. Cartelle and García-Gil, 2019).

The environmental evolution and sedimentary pattern of rivers through the Middle to Late Holocene have been widely studied over the Mediterranean area. For instance, in the Mediterranean and Black Sea,

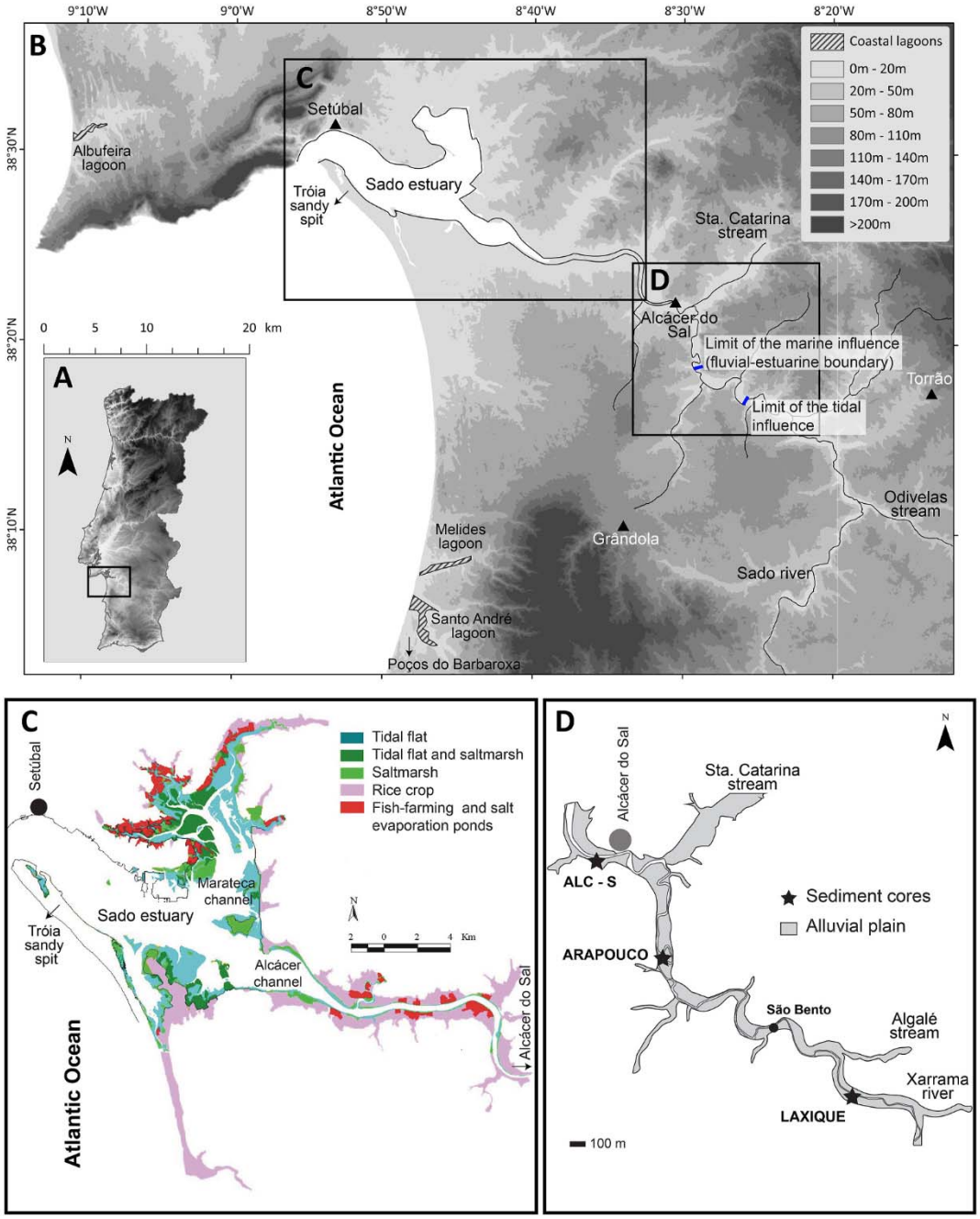

Fig. 1. Location of the study area. A - Location of the final ribbon of the Sado river and the Sado estuary in Portugal; B - Location of the present-day Sado estuary (C) and the studied area (D); C - Sado estuary with the morphosedimentary characterization of the marginal occupied areas (adapted from Andrade et al., 2006); D - Location of the sediment cores presented in this work.

where oceanographic conditions were favourable for the development and preservation of deltas, after the deceleration of sea level rise (at ca. 7500 cal BP followed by a further deceleration ca. 4000 cal BP; Vacchi et al., 2016) deltaic systems formed and evolved, showing changes in the progradation rates mostly depending on climatic forcing and anthropic pressure (e.g. Maselli and Trincardi, 2013; Anthony et al., 2014; Pleuger et al., 2019; Degeai et al., 2020). In South and Southwest Iberia, the combined scenario of low sea level rise rates (e.g. Vis et al., 2008; Leorri et al., 2012; Costas et al., 2016; García-Artola et al., 2018) and long-term drier climatic conditions (Fletcher et al., 2007, 2013; Carrión et al., 2010; Chabaud et al., 2014) prevailing during the Late Holocene, led to the retreat of marine influence, to the fill-in of the estuarine basins and to the expanse of tidal flats in estuarine areas (e.g. Dabrio et al., 2000; Camacho et al., 2016). At the Tagus, a bay-head delta developed following the decceleration of the sea level rise at ca. 7000 cal BP. Since that date onwards the progradation of the bay-head delta to further downstream areas took place, such as the fluvial environments (Vis et al., 2008).

Despite the available information on the environmental evolution and fluvial activity along the Mediterranean area, the record concerning Iberian rivers facing the Atlantic is still incomplete. Published data concerning the Holocene infilling of the Sado valley are scarce and essentially focused on the development of recent saltmarshes (e.g. Moreira, 1992; Psuty and Moreira, 2000). The aim of this work is to characterize the sedimentary pattern of the Sado river and its paleoenvironmental evolution over the Late Middle to Late Holocene (last 4500 cal BP), applying a multidisciplinary approach and the analysis of several environmental proxies determined in sediment samples collected from the present-day alluvial plain/saltmarsh areas, together with well-established chronological models. To accomplish this objective a high-resolution multi-proxy study (including texture, organic chemistry, nutrient content and diatoms) and chronological data was implemented in a sediment core collected in Laxique, ca. 65 km upstream the river outlet, in an area that is, nowadays, in fluvial domain. Data was complemented with paleoenvironmental and chronological information from sediment cores collected further downstream: Arapouco (Costa et al., 2019) and ALC-S (Moreira, 2016) (Fig. 1). Arapouco locates today near the fluvial-estuarine transition, considering the maximum salt-water intrusion until ca. 50 km from the river outlet (e.g. Bettencourt and Ramos, 2003) and considering information collected in 2017 on the present-day channel margin organic sediments (Costa et al., 2019). ALC-S was collected in the saltmarsh that develops in the left margin of the Sado estuary near Alcácer do Sal, in intertidal estuarine conditions (Moreira, 2016). The characterization of past environments relies on available data and environmental characteristics of present-day intertidal environments (present-day analogues).

The information retrieved from this study will contribute to improve the knowledge on the paleoenvironmental evolution of coastal lowlands from South Iberia during the Late Holocene, located in the westernmost areas affected by Mediterranean climatic conditions and facing the Atlantic Ocean. Knowing the behaviour of the fluvial-estuarine boundary and the fluvial sedimentary responses to past mean sea level (MSL) changes will, ultimately, contribute to estimate fluvial and estuarine responses to present and future MSL rise.

2. Study area

The Sado river is located in southwest Portugal (Fig. 1A). It is one of the greatest Portuguese rivers, with a maximum length of ca. 175 km and draining a wide watershed area with ca. 7700 km^2 (INE, 2007). It runs northward until the confluence with Odivelas stream (Fig. 1B) and further downstream it bends to northwest to its mouth, near the city of Setúbal (Fig. 1B). The river has a Mediterranean flow regime with instantaneous discharge of ca. 1 m^3 s^{-1} during the dry season and 50–80 m^3 s^{-1} during the rainy season that occasionally reaches 470 m^3 s^{-1} (Bettencourt and Ramos, 2003 and references therein), allowing for the flooding of alluvial plains margining the main channel. In natural conditions the mean annual flow was estimated to be 40 m^3 s^{-1}, but at present the river presents mean annual flows of ca. 7 m^3 s^{-1} under irregular hydrological regime conditions (Bettencourt and Ramos, 2003). It is characterized as a perennial river considering its flow intermittency and variability, being characterized by low inter-annual variability with very occasional zero-flow days (Oueslati et al., 2015). For comparison purposes, the average discharge of the Tagus river, the largest Iberian river located north of the Sado, is ca. 400 m^3 s^{-1} (e.g. Neves, 2010) presenting extreme seasonal and annual variability with flood peak discharges that sum-up to more than 30 times the mean flow, being influenced by Atlantic fronts that cross the Iberian Peninsula mostly during the winter (Benito et al., 2003).

The Sado presents a deep incised paleovalley, most probably resulting from multiple incisions during pre-Last Glacial Maximum (LGM) and, finally, during the LGM low-stands, that reaches ca. 40 m depth at Alcácer do Sal (GRID - Consultas Estudos e Projectos de Engenharia, 1989; ENGIVIA, n.d.) and ca. 38 m at São Bento (Fig. 1D) according to changes in depth of electric resistivity (Costa et al., 2020).

The terminal ribbon corresponds to a bar-built estuary occupying an area of about ca. 140–150 km^2 (Bettencourt and Ramos, 2003; Brito, 2009) with a mean depth of ca. 8 m, reaching 44 m near the inlet (Brito, 2009). The estuary is protected by the Tróia sandy spit (Fig. 1B and C), a sandy barrier that started to growth northwards ca. 6500 cal BP (Costas et al., 2015) progressively decreasing exchanges between the estuary and the sea. It reaches the Atlantic Ocean through a narrow inlet (ca. 2 km) between the north of the sandy barrier and Setúbal (Fig. 1B). According to Bettencourt and Ramos (2003) the estuary extends for a length of 50 km considering the maximum salt-water intrusion (herein considered as the fluvial-estuarine boundary) reaching the downstream limit of the studied area near Arapouco, or 57 km if the upper limit of dynamic tide is considered (Fig. 1B). Sado is a well-mixed mesotidal estuary (e.g. Martins et al., 2000; Biguino et al., 2021), with estuarine semi-diurnal tides, the tidal range varying between 1.5 m and 3.9 m during neap and spring tides, respectively (Bettencourt and Ramos, 2003). Wave weights in the estuary are usually lower than 1 m (Moreira, 1992).

The sediments deposited in the estuarine central basin correspond essentially to sand and muddy-sand, coarsening at the estuary mouth and in the main channels (e.g. Rodrigues, 1992). Finer sediments occur particularly in the marginal intertidal areas, where saltmarshes and tidal flats develop (e.g. Andrade et al., 2006, Fig. 1C). Rice plant crops, fish-farming and salt evaporation ponds occupy, nowadays, extensive marginal areas of the estuary (e.g. Andrade et al., 2006, Fig. 1C).

Considering the geological framework, the Sado river basin drains diverse formations, from rocks of the Precambrian and Palaeozoic Ages of the South Portuguese (SPZ - greenish and reddish colours) and Ossa Morena (OMZ - pinkish colours) Zones to Caenozoic deposits of Sado Basin (SB - yellowish colours; Fig. 2). In addition, Mesozoic sandstones, conglomerates, limestones and marls, outcropping at the Arrábida Mountain, occur north of the Sado estuary inlet (Geological Map of Portugal 1:500,000, synthetized by Brito, 2009, Fig. 2A).

In its initial course the Sado river crosses essentially shales and greywakes (Pimentel, 2002) and at a lesser extend limestones, quartzites, amphibolites and conglomerates (Geological Map of Portugal 1:500,000, from Serviços Geolgicos de Portugal, 1992 and synthetized by Brito (2009)) from the SPZ, and also metavolcanic rocks from the Iberian Pyrite Belt bearing massive sulphide pollymetalic deposits rich in magnetic particles (Pimentel et al., 2001; Matos and Oliveira, 2003). To northeast, crossed essentially by the right margin Sado tributaries, quartzite, quartzodiorites, shales and greywackes constitute the main lithologies outcropping from the OMZ, but dolerites, gabbros, metavolcanic and carbonated rocks are also present (Geological Map of Portugal 1:500,000, synthetized by Brito (2009), Fig. 2A).

On a closer scale, in the study area (Fig. 2B), the Sado channel is embedded essentially in sediments of the Paleogene Vale do Guizo

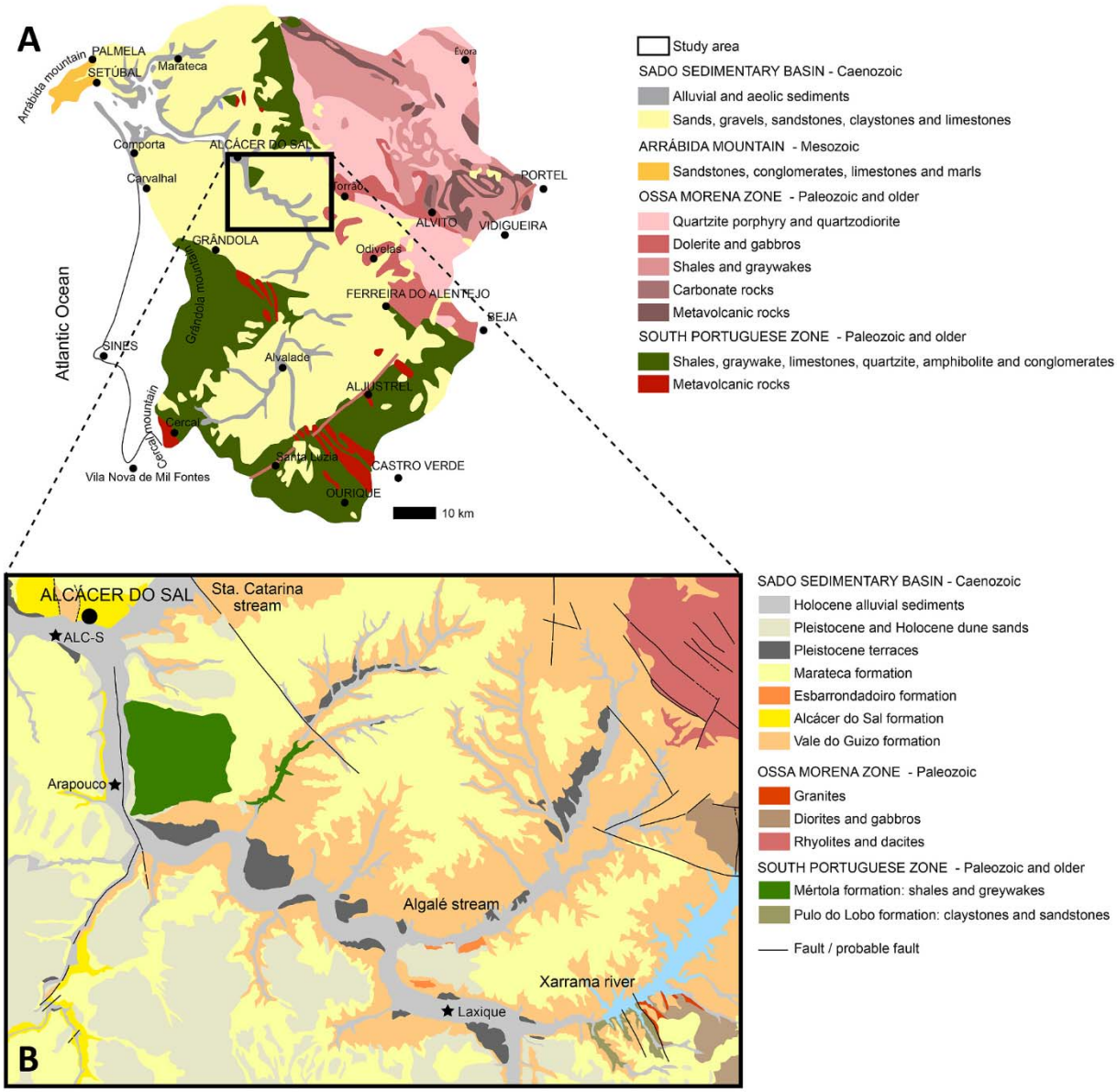

Fig. 2. Geological map of the Sado river basin. A - simplified lithological map of the Sado hydrological basin adapted from Brito (2009); B - geological map of the studied area adapted from Geological Map of Portugal 1:50,000 39-C, Alcácer do Sal (Antunes and Pais, 1991), and Geological Map of Portugal 1:50,000 39-D, Torrão (Antunes et al., 1991).

formation, constituted by alluvial pinkish sandy conglomerates and marly clays (Pimentel, 2002) and, between Arapouco and Alcácer do Sal, cuts sediments of the Miocene Alcácer do Sal formation composed by coastal yellowish biocalcarenites and marly sandstones (Antunes, 1983; Antunes and Pais, 1991; Antunes et al., 1991; Gonçalves and Antunes, 1992). Slaty pelitic rocks and greywackes of the Mértola formation (SPZ) outcrop in the right Sado margin near Arapouco (Fig. 2B; Antunes et al., 1991; Gonçalves and Antunes, 1992). Claystones and sandstones from the Pulo do Lobo formation (SPZ) and granites, diorites and gabbros (OMZ) are crossed by the Rio Xarrama tributary, at the proximity of its mouth in the Sado river (Antunes et al., 1991; Gonçalves and Antunes, 1992, Fig. 2B). The surroundings of the Sado valley and its tributaries, are covered by fluvial orange sands and clays of the Pliocene Marateca formation and by Pleistocene-Holocene aeolian quartz-rich sands remobilized from the Pliocene sediments, while Quaternary sandy terraces are present in both margins (Antunes et al., 1991; Gonçalves and Antunes, 1992, Fig. 2B).

3. Materials and methods

3.1. Sediment cores: collection and sampling

Laxique is a 10.5 m sediment core collected in the Sado alluvial plain, ca. 65 km upstream the Sado estuary inlet (Fig. 1; Table 1) at a height of 610 cm above MSL (from now onwards all depths are represented in height relative to present-day MSL) using a rotary core drilling with continuous sampling (CASABRANCA M3D equipment). The sediment core was collected in 7 sections with 150 cm each encapsulated in PVC tubes with 10 cm of diameter. Due to the coarser nature of the sediment below −200 cm MSL (810 cm depth) it was not possible to collect samples, despite the total depth of 1050 cm of the borehole. Topographic data (coordinates and altimetry) was obtained using Global Navigation Satellite Systems (GNSS) roving receiver units (Leica Geosystems models GPS 900 and NetRover) that operated in real-time, connected to Portuguese internet-based correction services.

Back in the laboratory, the core was opened, described and sub-

Table 1
Location and altimetry of the cores mentioned in this work. Coordinates are provided in ERTS89 TM06 Portugal coordinate system. Elevations are given relatively to mean sea level (MSL).

Core reference	Easting	Northing	Elevation of ground surface at core location (m *msl*)	Start collection point (m *msl*)	End collection point (m *msl*)	Collected core length (cm)	First published in
ALC-S	−33471.69	−143995.7	1.5	1.5	−1.2	270	Moreira, 2016
Arapouco2	−31026.1743	−149671.94	2.2	2.2	−0.48	268	Costa et al. (2019)
Arapouco3	−31030.6767	−149673.241	2.2	0.2	−4.70	490	Costa et al. (2019)
Laxique1	−21174.326	−157053.121	6.1	6.10	−2.00	810	This work

sampled in 2 by 2 cm samples. Sediment sub-samples were subsequently freeze-dried, split and homogenized representative quantities were disaggregated and grinded using an agate mortar for chemical and compositional analysis (see below).

To characterize the Sado valley Late Holocene sedimentary infilling and its evolution, data from other sediment cores recovered river downstream (Fig. 1D) have been collected (Table 1). Arapouco is a ca. 7 m-long sediment core collected in the alluvial plain of the Sado river, located at the present-day fluvial-estuarine boundary (Fig. 1D). The sediment is mainly constituted by grey mud to slightly sandy mud (units 2 to 5; max. sand content of 15%; detailed description in Costa et al., 2019), deposited above a coarse sediment (unit 1) constituted by heterometric sand, mainly composed by angular to sub-angular hyaline and milky quartz and mica grains. Briefly, units 2, slightly coarser, and 3, present low magnetic susceptibility (MS) values, high contents of organic material (8%), mean $\delta^{13}C$ values of −24‰ and mean C/N values of 12 pointing to the predominance of organic material sourced in marine components. In addition, whole shells of *Scrobicularia plana* were found among the sediment. The diatom record is mainly composed by marine to marine/brackish planktonic taxa (such as *Paralia sulcata* and/or *Actinoptychus senarius*) in unit 2, while in unit 3 it is almost exclusively composed by marine planktonic diatoms (as *Thalassiosira* species). In unit 4, the MS increases at regular spaces, total organic matter has mean values of 8.4%, $\delta^{13}C$ varies between −24.5 and −26‰ decreasing upwards and C/N values present an increasing tendency from values of 12 at the base to values of 14 at the top. The diatom record shows an upward transition characterized by marine, marine/-brackish and brackish/freshwater diatoms (*Cocconeis* spp. and *Nitzschia* spp. as dominant species). Unit 5, deposited above MSL, is characterized by MS peaks, increase in the sand content upwards, decrease in the total organic matter content, low organic carbon values and $\delta^{13}C$ values varying between −25 and −27‰. In this unit, the diatom record is composed only by fragments. According to the previous interpretations (Costa et al., 2019), the sedimentary pattern reflects deposition under intertidal conditions until ca. 3240 cal BP (units 2 to 4) and consequent aggradation of the alluvial plain (unit 5).

ALC-S is a 2.2 m-long sediment core, collected in the left intertidal margin of the Sado estuary near Alcácer do Sal (Fig. 1D). Sediments are mainly constituted by grey mud to slightly sandy mud, with brownish colours at the top 70 cm (Moreira, 2016). The base of the core represents accumulation in a tidal flat environment that evolved at the top to a saltmarsh that continues to grow at present in the area (Moreira, 2016).

3.2. Radiocarbon dating and age-model

Four bulk organic sediment samples at different depths were selected for AMS radiocarbon dating and processed at Beta Analytic (USA) laboratories. Radiocarbon ages were calibrated using Oxcal 4.4 (© Bronk Ramsey, 2020) and the IntCal20 (Reimer et al., 2020) calibration curve. Post-bomb dates were calibrated using the NH zone 2 curve (Hua et al., 2013). Sedimentation rates were determined using the CLAM 2.3.2 (Blaauw, 2010). Best-fit ages determined based on sedimentation rate curves were used as chronological indicators.

3.3. Magnetic susceptibility and texture

Volume magnetic susceptibility (MS) was measured in SI units directly over the core at every 2 cm using a Bartington® MS2 instrument equipped with a MS2E sensor at Instituto Hidrográfico.

A representative portion of the total sediment samples was washed through a 63 μm-mesh sieve and the fraction >63 μm was weighted to determine the percentage of coarse (CF) and fine (FF) fractions. Sediment was classified according to Flemming (2000). The coarse sample collected between 805 and 810 cm was sieved in a normalized series of ASTM sieves between 4 φ and −4 φ with an interval of 0.5 φ. Samples were characterized following Folk (1954) using the software GRADISTAT (Blott, 2000). Composition and morphoscopic characteristics were described using a Leica MZ12 binocular stereomicroscope.

Micro Fourier-transformed infrared spectroscopy (μ-FTIR) comprised of a Bruker Hyperion 3000 IR microscope with a mercury-cadmium-telluride detector (MCT) for MIR measurements, controlled by OPUS 7.2 software (2012) © Bruker Optik GmbH, was carried out at HERCULES Laboratory on a plastic fragment found at ca. 25 cm core depth in order to identify the material. Transmission measurements were performed using a 15 × magnification objective and a micro-compression diamond cell EX'Press 1.6 mm, STJ-0169. Spectra were recorded with 4 cm^{-1} resolution using 64 co-added scans.

3.4. Organic matter and organic material sources

Total organic matter content (OM) was determined following Kristensen (1990) adapted method *Loss on ignition* (LOI): milled sub-samples were heated in a muffle furnace at 520 °C for 12 h and OM determined by weight difference.

Total organic carbon (% C_{org}), total nitrogen (% N), $\delta^{13}C_{VPDB}$ and $\delta^{15}N_{AIR}$ were determined in ground sub-samples after removal of inorganic carbon using HCl 10% at *Servizos de Apoio a Investigación*, University of A Coruña (UDC), Spain. Samples were homogenized and weighed in tin capsules. Capsulated samples were analysed with a FlashEA1112 combustion elemental analyser (ThermoFinnigan) coupled on−line with a Delta Plus Finnigan MAT Isotope Ratio Mass Spectrometer. All carbon and nitrogen isotope ratios are expressed in conventional δ notation: $\delta^{13}C_{VPDB}$ and $\delta^{15}N_{AIR}$ calculations are given as $[(R_{sample} - R_{standard})/R_{standard}]*1000$, where R_{sample} and $R_{standard}$ are the $^{13}C/^{12}C$ or $^{15}N/^{14}N$ isotope ratios of the sample and standard, respectively. The $\delta^{13}C$ isotope ratio of samples was determined by comparison with a CO_2 reference gas standard (99.996%, $\delta^{13}C_{VPDB} = -6.317$) and values are reported relative to Vienna Pee Dee Belemnite (VPDB) standard. $\delta^{15}N$ values are referred to air.

To differentiate the proportion of particulate organic materials derived from marine and freshwater algae and from terrestrial vascular plants the formula described by Alonso-Hernandez et al. (2007) was applied. To distinguish between organic carbon from freshwater and marine sources the equation described in Schultz and Calder (1976) was used.

3.5. Nutrients

Nutrient contents in shallow coastal areas rely on allochthonous fluvial loads and on autochthonous nutrient cycling (e.g. Slomp, 2011; Scanes et al., 2017). Nutrient cycling is highly dependent on diverse physical forcing factors such as temperature, salinity, light, tidal currents, biological activity, among others (e.g. Henriksen and Kemp, 1988; Herbert, 1999; Scanes et al., 2017) and thus its influence on the palaeoecological record is difficult to access and should be taken with care (e.g. Scanes et al., 2017). Estuarine water nutrients, particularly nitrogen (N) and phosphorus (P), are limiting factors for biological productivity. Its contents are mostly dependent on inputs from the catchment area and its availability sustained by internal nutrient recycling where nutrient remineralisation in the sediment-water interface plays a major role (e.g. Henriksen and Kemp, 1988; Scanes et al., 2017). Nutrients and nutrient cycling are also affected by anthropic landscape manipulation (e.g. Slomp, 2011), so nutrient variations with depth can improve our knowledge on the anthropogenic influence in riverine/estuarine systems (e.g. Scanes et al., 2017).

In the present work, sulphate is used as a proxy for the influence of marine water since it is a conservative element in sea and estuarine water and its concentration varies depending on salinity (e.g. Marino and Howarth, 2009).

Nitrate, phosphate, total phosphorus and total sulphate were determined at the AmbiTerra laboratory from the University of Évora. Nitrate (NO_3^-; mg/kg) content was carried out with a nitrate selective electrode (model ISE 31 B) in a Consort multi-parameter analyser (model C863). The extracting solution was ISA solution $(NH4)_2SO_4$ 2 M) with a ration 2 g sample: 10 mL ISA.

Total phosphates (PO_4^{3-}) were determined on ignited samples (2 h at 550 °C), followed by acid extraction through shaking samples with 1 N H_2SO_4 for 16 h (Pansu and Gautheyrou, 2006). Phosphate contents were determinate by UV visible spectrophotometry (Thermo Scientific, Evolution 201), following the ascorbic acid – ammonium molybdate method (Murphy and Riley, 1962). The accuracy and analytical precision of all the analysis have been checked using analyses of duplicate samples in each analytical set.

Total content of Phosphorus (P) was determined in samples melted with an alkaline flux of Spectroflux 100 B (tetraborate and lithium metaborate) in pure graphite crucibles in a muffle furnance at 1000 °C followed by dissolution in a nitric solution. Phosphorus was analysed by optical emission spectroscopy with inductive plasma source (ICP-OES, PerkinElmer OPTIMA 8300), operated under the following conditions: plasma gas flow - 10 L/min; auxiliary gas flow - 0.2 L/min; nebulizer gas flow - 0.70 L/min; sample flow - 1.50 mL/min; RF Power - 1450 W; viewing modes - radial and axial; reading time - 2–5 min; read delay - 80 s; normal resolution; internal standard – yttrium. For quality control, this analytical procedure was tested with analytical replicates, two blanks prepared using the same analytical methods and Certified Reference Materials (CRMs) with an accuracy of R<5%: NIM-L (MINTEK, South Africa), JR-3 and JA-2 (GSJ, Japan), GSR-1 and GSR-5 (IGGE IRMA, China). Multi-element Quality Control (QC) solution accounted for less than 2% and CRMs were run every 10 samples.

Determination of sulphate ion (SO_4^{-2}) followed the method described by Singh et al. (2011): sulphate was extracted by an acidified ammonium acetate solution and converted to a $BaSO_4$ suspension under controlled conditions. The resulting turbidity was measured by molecular absorption spectrophotometry at a wavelength of 420 nm on a Thermo Scientific (Evolution 201) spectrophotometer, using a K_2SO_4 solution as standard.

3.6. Diatoms

For diatom identification, samples (0.01 g dry weight) were processed according to standard techniques (Renberg, 1990). Cleaned subsamples were dried onto coverslips and mounted onto microscope slides with Naphrax (RI = 1.74). Identification was undertaken with a magnification of 1000× using a Nikon Eclipse 600 microscope with Nomarski differential interference contrast optics. A minimum of 300 valves were counted per sample. Interpretation was based on the diatom species (with relative abundances equal to or higher than 5% in at least one sample), environmental preferences (salt, brackish or fresh water), habitat and lifeform (benthic, thycoplanktonic or planktonic), following Vos and de Wolf (1993).

4. Results

4.1. Chronology and age-models

Table 2 shows results obtained from radiocarbon dating for different cores collected in the Sado channel, Laxique, Arapouco and ALC-S. All radiocarbon dates fall within the Middle-Late Holocene transition and Late Holocene, reflecting the sedimentary pattern and changes occurred in the last 4500 years (Table 2).

Fig. 3 presents the age-models draw for Laxique, Arapouco (Costa et al., 2019) and ALC-S, based on the radiocarbon dates.

The Arapouco age-model was published and discussed in Costa et al. (2019). Briefly, mean SR of 2.2 cm yr^{-1} were determined for the interval between ca. 3600 cal BP (−425 cm MSL) and 3232 cal BP (at a depth corresponding to the present-day MSL) and mean SR of 0.06 cm yr^{-1} were calculated for the last 3230 years (above MSL until the top of the core located at 220 cm MSL; Fig. 3).

The age-model draw for ALC-S was based on only two radiocarbon dates (Table 2) and should be looked cautiously; however a similar sedimentation pattern was found with high SR of 2.4 cm yr^{-1} between 680 and 600 cal BP (the base of the core at ca. −120 cm MSL and 80 cm MSL), and a SR of 0.12 cm yr^{-1} for the last 600 years (Fig. 3; age-model adapted and updated from the one published in Moreira, 2016). Likewise, in Laxique, despite lower than the ones determined for Arapouco and ALC-S, higher sedimentation rates of 0.75 cm yr^{-1} were determined for the interval between 4400 cal BP (at the core base) and 4000 cal BP (90 cm MSL) and lower sedimentation rates of ca. 0.07 cm yr^{-1} were calculated for the sedimentary column between 4000 and 970 cal BP (290 cm MSL; Fig. 3) from where SR increases to values of 0.17 cm yr^{-1} until ca. 1950 AD (460 cm MSL). In the last 150 cm, very high SR of 2.5 cm yr^{-1} were determined, but this value can somehow be affected by agriculture procedures. According to the model settings, the goodness of fit was 4.3 despite the short number of available dates (4) and the model was accepted. Ages and uncertainty ranges for each date were calculated for each cm and best-fit dates were used for the presentation of the results and interpretations.

4.2. Texture and composition: multi-proxy analyses from the Laxique sedimentary succession

Laxique is a sediment core mostly constituted by grey to brown sandy mud (CF between 20% and 40%), slightly sandy mud and mud (CF lower than 20%; Fig. 4A) excepting the basal sample (−195 to −200 cm MSL), characterized as sandy gravel (63% gravel, 37% sand and negligible amounts of mud; following Folk, 1954, Fig. 4D). The coarse fraction is essentially constituted by quartz, with very rare to slightly abundant heavy minerals and micas (biotite and muscovite). Changes in the coarse fraction composition are described below. Very rare to rare macroplant remains (e.g. wood fragments, seed, fibres, spores) are present in all samples.

The gravel and sand components of the basal sample are constituted by angular centimetric clasts containing essentially quartz and quartzite and, at a lesser extent, by shale, granite, greywacke and sandstone, among other less representative rock materials. Despite only the top 5 cm sediment of this coarse unit were sampled and no other analyses were performed, a basal Unit 0 was established, at least between −440 m and −195 m MSL, until where the corer sample drilled. The ERT profile

Table 2
Radiocarbon determinations in organic sediment for the cores used in this work. The dates have been calibrated with the IntCal20 curve (Reimer et al., 2020) using the Oxcal v.4.4 (© Bronk Ramsey, 2020) and the NH zone 2 curve (Hua et al., 2013)*.

Sample reference	Lab code	Material	Core depth (cm)	Height (cm MSL)	$\delta^{13}C$ (‰)	Conventional ^{14}C age BP	Calibrated age BP (95%)	Reference
Laxique1 150–152*	Beta-510626	Bulk organic sediment	151	459	−24.9	101 ± 0.38pMC*	−6 to −7	This work
Laxique 320-322	Beta-482231	Bulk organic sediment	321	289	−25.8	1060 ± 30	1056-1024 (16.8%) 1007-926 (78.6%)	This work
Laxique1 521-523	Beta-51062	Bulk organic sediment	522	88	−26.0	3670 ± 30	4090-3900 (95.4%)	This work
Laxique 801-803	Beta-476962	Bulk organic sediment	802	−191	−25.9	3940 ± 30	4515-4480 (10.2%) 4445-4289 (82.8%) 4270-4254 (2.5%)	This work
Arapouco2#9 152-154	Beta-436176	Bulk organic sediment	153	67	−25.4	2620 ± 30	2776-2721 (95.4%)	Costa et al. (2019)
Arapouco2#10 200-202	Beta-408535	Bulk organic sediment	201	19	−25.4	3170 ± 30	3454-3346 (95.4%)	Costa et al. (2019)
Arapouco3#2 354-356	Beta-393523	Bulk organic sediment	355	−135	−22.7	3100 ± 30	3383-3227 (95.4%)	Costa et al. (2019)
Arapouco3#4 552-554	Beta-408534	Bulk organic sediment	553	−333	−23.5	3400 ± 30	3815-3801 (2.0%) 3718-3564 (93.4%)	Costa et al. (2019)
Arapouco3#5 624-627	Beta-431370	Bulk organic sediment	625.5	−405,5	−23.4	3210 ± 30	3468-3371 (95.4%)	Costa et al. (2019)
Arapouco3#5 635-637	Beta-431371	Bulk organic sediment	636	−416	−23.5	3330 ± 30	3636-3466 (95.4%)	Costa et al. (2019)
ALC-S S1 0.78–0.79	Beta-417791	Bulk organic sediment	78.5	72	−23.2	610 ± 30	651-546 (95.4%)	Moreira, 2016
ALC-S S1 2.68–2.69	Beta-417792	Bulk organic sediment	268.5	−118	−25.6	740 ± 30	725-652 (95.4%)	Moreira, 2016

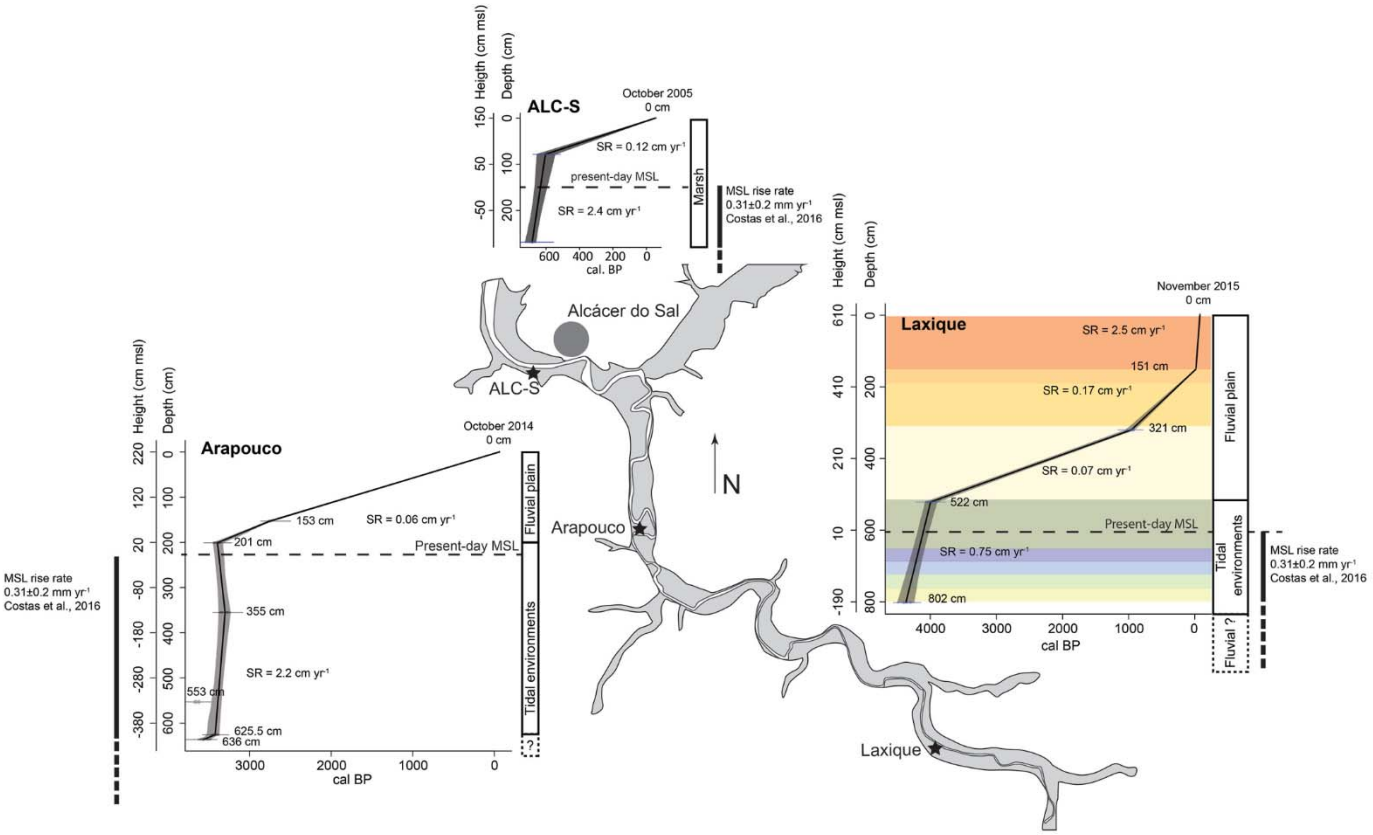

Fig. 3. Sedimentation rates (SR) determined for the sediment cores Laxique, Arapouco (Costa et al., 2019) and ALC-S (age-model updated from the one published in Moreira, 2016). For description of the units, represented by the different colours for Laxique, see the section below. (For interpretation of the references to colour in this figure legend, the reader is referred to the Web version of this article.)

performed near Laxique is consistent with the existence of coarse material in depth (Mota, 2017). However, deep boreholes crossing the infilling are needed to confirm this hypothesis.

Above −195 cm, changes in depth in all the analysed proxies were identified and based on these changes Laxique was divided in 6 main sedimentary units, which were subdivided in smaller subunits when

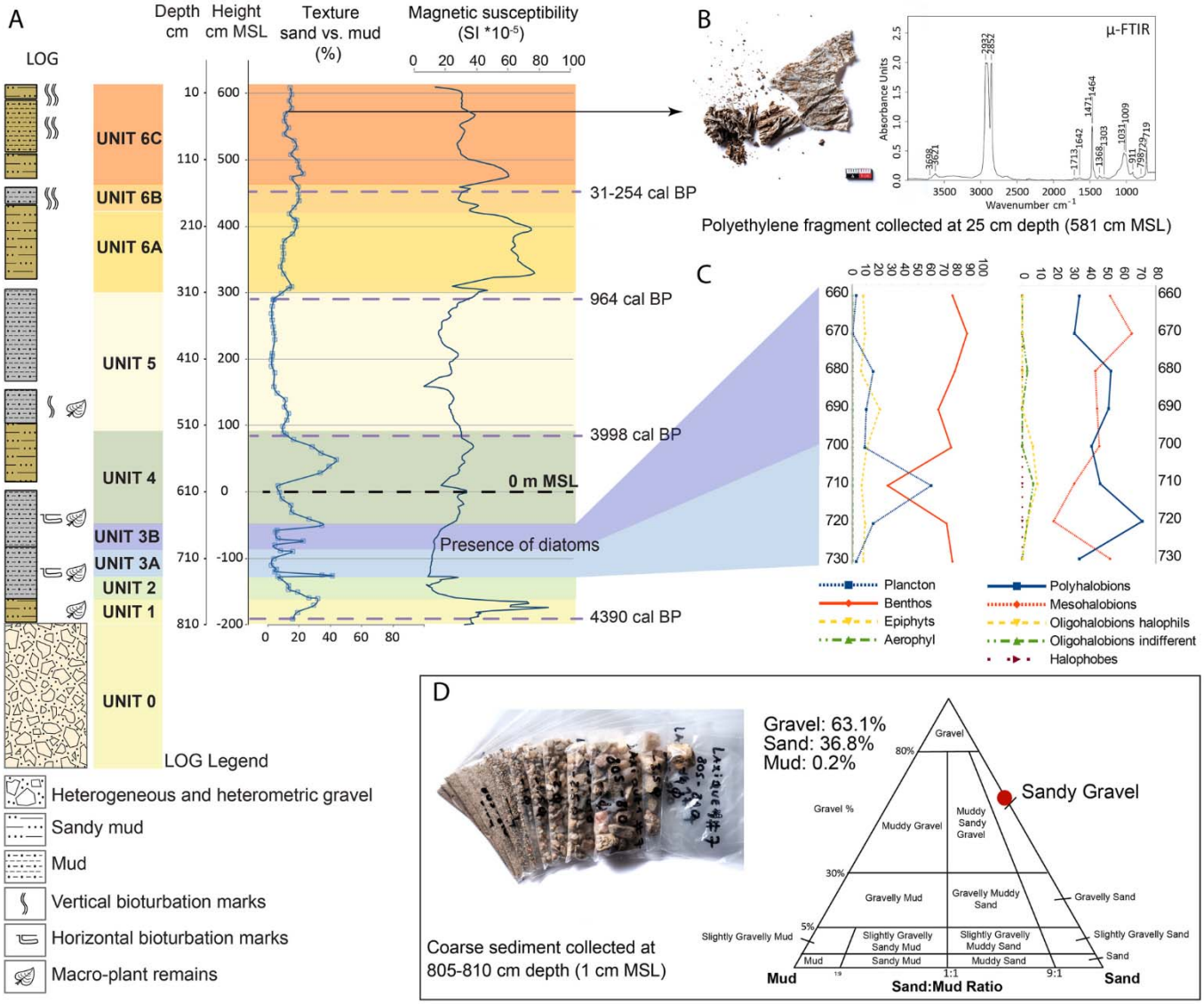

Fig. 4. Representation of the different sedimentological units identified in Laxique. A - LOG and representation of texture (sand *vs.* mud) and magnetic susceptibility (MS) against depth below surface and height, with identification of the depth where the plastic fragment was collected (25 cm core depth). B - Plastic fragment photo and μ-FTIR analyses graph reflecting its components (polyethylene); C - Down-core distribution (between −50 and −120 cm MSL; 660 and 730 cm core depth) of diatom assemblages. D - Photo of the sample collected between −200 and −195 cm MSL separated by φ and ternary-plot gravel-sand-mud with representation and classification of the sample collected at the core base, following Folk (1954). Photos © José Vicente | Agência Calipo.

necessary, due to profile changes in one or more proxies (Figs. 4–6). Sedimentary statistic parameters are presented in Table 3.

Unit 1 (between −195 cm and −160 cm MSL) is constituted by brown slightly sandy mud coarsening upwards to a sandy mud associated with a peak in the MS between −187 and −161 cm MSL reaching values of 86 × 10^{-5} SI (Fig. 4A; Table 3). The sand content may, in part, be associated with bioturbation (described while sampling). Most quartz grains present clean surface, but some show orange colours related to Fe coating. The OM content is low which is consistent with the low contents of C_{org} and N and the C/N ratio presents constant values around 10 (Figs. 5 and 6). The $\delta^{13}C$ and the $\delta^{15}N$ reflect a freshwater/terrestrial source for the organic material (Figs. 5 and 6; Lamb et al., 2006; Khan et al., 2015).

Unit 2 with only 30 cm height (between −160 and -130 cm MSL) is marked by abrupt changes in several analysed proxies. This unit is characterized as a slightly sandy mud with low contents of coarse materials. In the coarse fraction, very rare to rare fibrous gypsum grains occur. Magnetic susceptibility is low (Fig. 4A) with the maximum MS values recorded at the top of the unit, reaching 27 × 10^{-5} SI at −130 cm MSL. Total OM, C_{org} and N increase in relation to Unit 1, as well as the C/N ratio (Figs. 5 and 6; Table 3). Notwithstanding, $\delta^{13}C$, $\delta^{15}N$ and nutrients have similar values to Unit 1, with the NO_3^- presenting the highest values of the sedimentary succession, above 90 mg kg^{-1} (Fig. 6).

Unit 3 (between −130 and −50 cm MSL) was primarily identified due to the presence of diatoms (Fig. 4C) and higher contribution of marine compounds to the particulate organic carbon (Fig. 5). It presents low MS response (Fig. 4A), low $\delta^{13}C$ and $\delta^{15}N$ values and C/N ratio ca. 12. $\delta^{13}C$, C/N and OM decrease progressively upwards, whereas $\delta^{15}N$ content is almost constant (Figs. 5 and 6). However, the results of the subsequent analyses made possible to distinguish two different subunits. **Sub-unit 3A** (between −130 and −90 cm MSL) is constituted by sandy mud at the base and mud to the top (the content of the CF increasing to ca. 15% in the top sample) with low content in particles susceptible to magnetize (Fig. 4A). Rare quartz grain surfaces present iron oxide coating (FeO) and iron oxide minerals were identified in the base samples as well as gypsum crystals and fibrous and nacreous

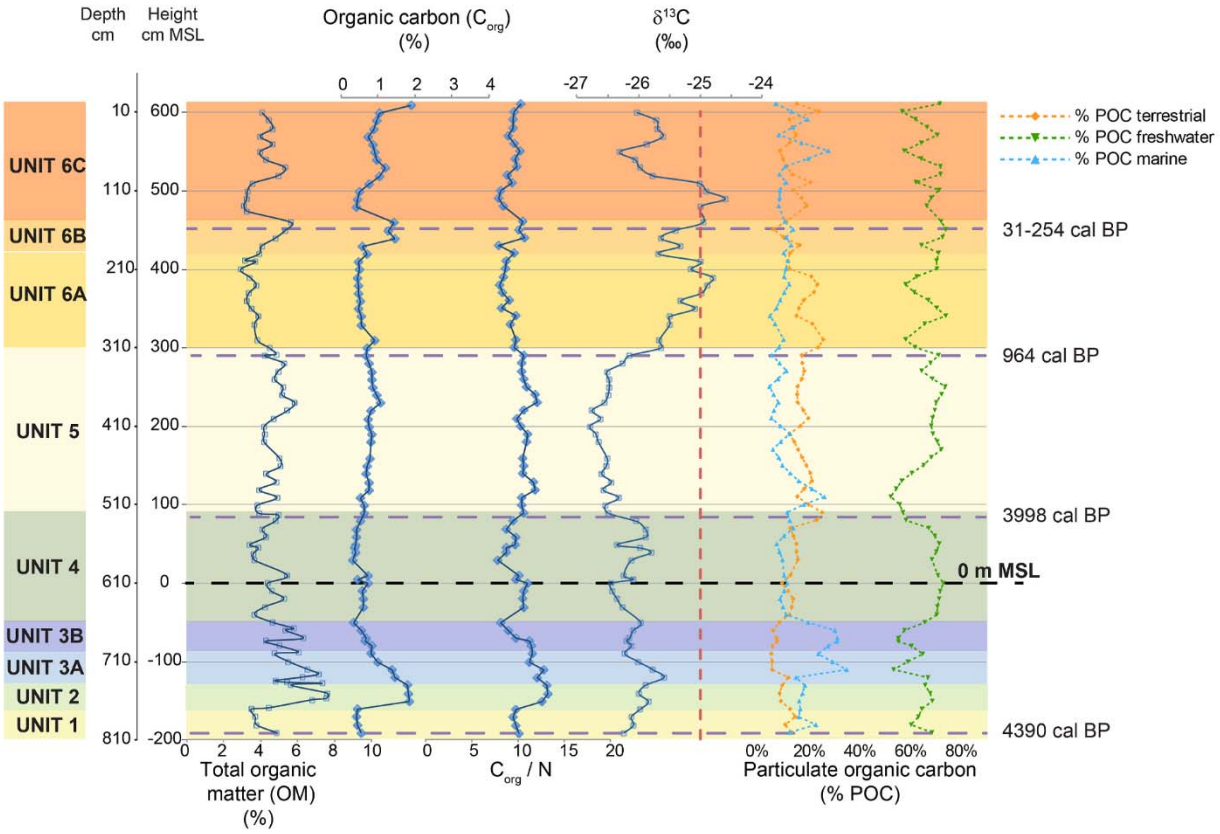

Fig. 5. Representation of the sedimentological and organic analysed proxies against depth below surface and height: total organic matter (OM), organic carbon (C_{org}), C/N, $\delta^{13}C$ and particulate organic carbon (POC) with terrestrial, freshwater and marine origin (Alonso-Hernandez et al., 2007).

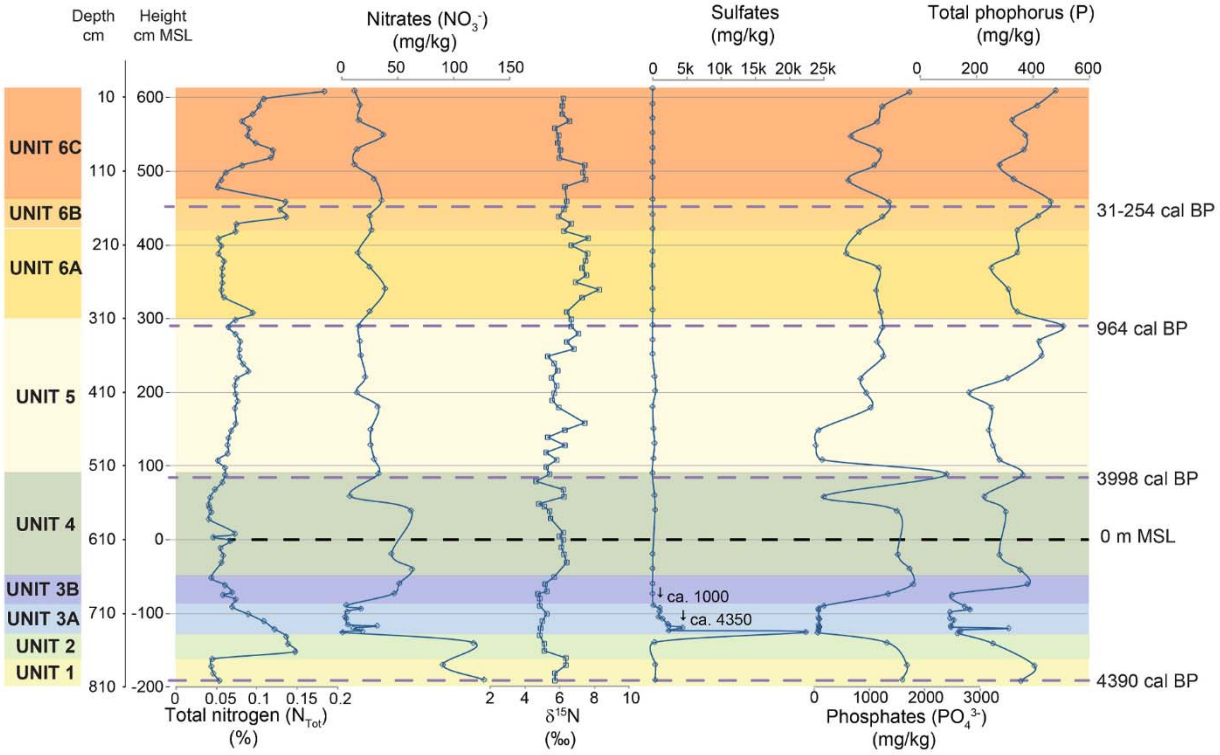

Fig. 6. Representation of the nutrients against depth below surface and height: Total nitrogen (N), nitrates (NO_3^-), $\delta^{15}N$, sulphates (SO_4^{-2}), phosphates (PO_4^{-3}) and phosphorus (P).

Table 3
Sedimentological and chemical statistic parameters of the defined units (Costa et al., 2021).

			CF (%)	MS $\times10^{-5}$ SI	OM (%)	N (%)	$\delta^{15}N$ (‰)	C_{org} (%)	$\delta^{13}C$ (‰)	C/N	NO_3^- (mg kg^{-1})	PO_4^{-3} (mg kg^{-1})	P (mg kg^{-1})	SO_4^{-2} (mg kg^{-1})
UNIT 6	SU-6C	average	14.8	35.6	4.2	0.10	6.4	0.90	−25.6	9.3	19.5	1101.3	366.5	70.8
		max.	21.8	60.5	6.7	0.18	7.5	1.89	−24.6	10.3	37.3	1731.6	480.4	106.6
		min.	10.1	13.7	3.1	0.05	5.7	0.43	−26.3	8.0	11.7	624.3	279.6	32.4
	SU-6B	average	17.1	38.2	4.5	0.11	6.3	1.09	−25.4	9.8	29.2	1145.0	406.2	111.6
		max.	19.2	61.3	5.6	0.14	6.7	1.46	−25.0	10.8	35.7	1354.4	460.4	141.8
		min.	13.2	28.2	3.1	0.07	5.9	0.59	−25.7	7.9	25.3	828.3	342.6	73.4
	SU-6A	average	11.1	62.0	3.7	0.06	7.2	0.55	−25.2	8.9	23.9	1072.6	350.2	65.6
		max.	17.9	76.7	4.8	0.09	8.3	0.93	−24.8	9.8	38.7	1249.5	505.5	103.6
		min.	3.6	30.6	2.9	0.05	6.4	0.45	−25.7	8.1	14.8	590.6	250.4	19.8
UNIT 5		average	5.0	22.9	4.7	0.07	6.0	0.78	−26.5	10.8	22.9	692.5	295.4	252.1
		max.	12.5	32.7	5.8	0.09	7.4	1.08	−26.2	12.0	32.8	1261.9	428.1	535.8
		min.	1.9	6.6	3.8	0.05	5.2	0.54	−26.8	9.9	13.6	46.3	173.1	59.6
UNIT 4		average	21.4	30.4	5.3	0.05	5.7	0.50	−26.2	9.6	42.1	1472.2	304.4	218.4
		max.	43.2	37.9	5.4	0.07	6.4	0.74	−25.8	11.0	63.2	2404.3	362.0	431.7
		min.	5.9	17.5	3.4	0.04	4.6	0.32	−26.5	7.8	7.7	181.4	225.2	28.6
UNIT 3	SU-3B	average	11.8	15.2	5.3	0.06	5.1	0.62	−26.1	9.9	49.0	1569.6	245.5	64.9
		max.	34.0	21.1	6.3	0.07	5.7	0.84	−26.0	11.5	51.4	1798.8	379.3	66.5
		min.	3.6	12.6	4.3	0.04	4.7	0.36	−26.2	8.1	46.6	1340.5	111.7	63.2
	SU-3A	average	13.6	13.2	6.0	0.10	5.0	1.16	−25.9	11.9	10.6	101.4	146.8	3885.7
		max.	40.5	8.8	7.3	0.12	5.2	1.46	−25.6	12.8	31.4	193.3	311.2	22430.6
		min.	1.9	28.2	4.8	0.07	4.9	0.80	−26.2	11.3	0.8	69.0	107.2	215.8
UNIT 2		average	15.2	15.1	6.9	0.14	5.0	1.82	−25.9	13.0	117.8	1332.2	257.5	403.9
		max.	25.35	26.6	7.6	0.15	5.1	1.86	−25.9	13.2	117.8	1332.2	257.5	403.9
		min.	7.2	7.7	5.6	0.14	4.9	1.79	−26.0	12.6	117.8	1332.2	257.5	403,90
UNIT 1		average	23.5	49.8	4.1	0.05	6.0	0.46	−26.1	9.8	108.6	1644.0	380.8	488.5
		max.	31.2	85.8	4.9	0.05	6.4	0.55	−26.0	10.2	126.9	1685.6	404.3	541.2
		min.	15.4	32.4	3.5	0.04	5.7	0.41	−26.2	9.5	90.3	1602.4	357.3	435.9

gypsum grains. Heavy minerals increase to the top. Charcoal fragments only occur in the top samples. The Sub-unit is marked at the base by a sharp peak in the concentration of SO_4^{-2} that reaches values of 22,430 mg kg^{-1} at −128 cm MSL (Fig. 6), being the concentration of SO_4^{-2} always high within this sub-unit despite decreasing progressively upwards (Fig. 6), similarly to other compounds. The high contents of SO_4^{-2} are probably related to the presence of gypsum crystals. Conversely, the contents of NO_3^-, PO_4^{-3} and P present the lower contents of all the entire sedimentary succession, with the lower concentration of NO_3^- and PO_4^{-3} coincident with the peak the sulphates (Fig. 6). Despite the low contents of P, a peak occurs at −120 cm MSL with values of 310 mg kg^{-1}. **Sub-unit 3B** (between −90 and −50 cm MSL) is characterized as slightly sandy mud, and sandy mud at the very top, according to its contents in coarse sediments (Fig. 4A). In coarse fraction quartz grains present clean surfaces. Iron oxide minerals occur at the top samples. SO_4^{-2} decreases one order of magnitude to mean values of 66 mg kg^{-1}. Phosphorus has low values at the base but increases to values of 330 mg kg^{-1} at the top of the Sub-Unit (Fig. 6). The dominant diatoms at Sub-unit 3A are polyhalobious diatoms mostly with a planktonic life form such as *Cymatosira belgica*, *Thalassionema nitzschioides*, *Thalassiosira eccentrica* which are later replaced in Sub-unit 3B by benthic species like *Tryblionella navicularis* and *Navicula incerta* with lower salinity preferences (Fig. 7).

Unit 4 (between −50 and 88 cm MSL) has variable contents in the CF being characterized as mud until ca. 9 cm MSL, and as slightly sandy mud and sandy mud to the top where MS presents slightly higher values. This Unit is characterized by the presence of very rare to rare calcite grains in the coarse fraction at the base and abundant calcite grains at the top near the transition to Unit 5. In addition, FeO minerals are slightly abundant to abundant. Total OM has a decreasing trend to the top and the maximum values of C_{org} and N (0.7% and 0.07%, respectively at 4 and 9 cm MSL) are coincident with the higher contents of OM (Figs. 5 and 6). Similarly to the Units below, $\delta^{13}C$ has values of −26‰ while $\delta^{15}N$ varies between 6.4 and 4.6‰. C/N ratio ranges between 11 and 7.8 (Fig. 5). The concentration of NO_3^-, PO_4^{-3} and P are similar to Sub-unit 3B, but decrease at the top of the Unit (Fig. 6). However, the transition to Unit 5 is marked by an increase in the PO_4^{-3} and P contents that reach concentrations of 2400 mg kg^{-1} and 360 mg kg^{-1}, respectively. Sulphates decrease to very low values of 28 mg kg^{-1} at the top of the Unit (Fig. 6).

Unit 5 (between 88 and 289 cm MSL) is composed by very fine sediments (mud) with low contents of CF and low MS values despite the slightly coarser sediments at the base between 88 and 148 cm MSL with CF mean values of 10% (sandy mud) (Fig. 4A). In coarse fraction quartz grains are coarser than in the units below. Some grains present orange surface due to Fe coating. Iron oxides and orange sandstone fragments were identified above 400 cm (i.e. 210 cm MSL) and slightly abundant ore slag fragments were also identified in the samples above 362 cm (i.e.

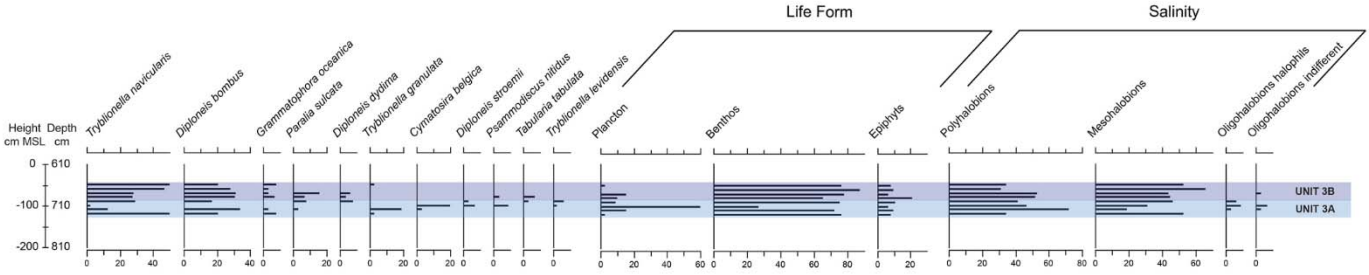

Fig. 7. Diatom taxa, life form and salinity in Sub-units 3A and 3B.

250 cm MSL). The OM content has mean values of 4.7%, C_{org} presents mean contents of 0.8% with a maximum value of 1.1% at 230 cm MSL and N shows mean values of 0.07%. The C/N ratio varies between 12 and 9.9, presenting slightly higher values than the Unit 4. $\delta^{13}C$ has the lower values of all the sedimentary succession, always lower than −26‰ and $\delta^{15}N$ varies between 7.4 and 5.2‰, with the higher value measured at 160 cm MSL. Sulphates vary between 150 mg kg^{-1} at 180 cm MSL and 536 mg kg^{-1} at 200 cm MSL, decreasing to the top of the Unit to values lower than 80 mg kg^{-1}. The concentration of NO_3^- is low, below 33 mg kg^{-1}. Phosphates concentration range between 150 and 46 mg kg^{-1} from the base of the Unit until ca. 150 cm MSL, increasing to high values of 1261 mg kg^{-1} upwards. Phosphorus has a diminishing tendency until 200 cm MSL, from where it starts to increase reaching values of 430 mg kg^{-1} at the top of the Unit. No signs of bioturbation were identified while sampling.

Unit 6 corresponds to the top 3 m of the core deposited during the last ca. 1000 years (between 289 and 610 cm MSL; Fig. 3). The Unit was divided in three sub-units based on changes in several proxies, particularly MS, C_{org}, N and $\delta^{13}C$ (Figs. 5 and 6). In general, OM decreases in relation to the Units below and nitrates are almost constant over the Unit presenting low values resumed in Table 3.

Sulphates present values lower than 140 mg kg^{-1}. **Sub-unit 6A** (between 289 and 410 cm MSL) is composed by a slightly sandy mud with relative high values of MS ranging between 30–40 × 10^{-5} at the base (ca. 289–310 cm MSL) and between 50–77 × 10^{-5} between 310 and 410 cm MSL. The C_{org} and N contents decrease from maximum values of 0.9 and 0.09% at the base and minimum values of 0.5 and 0.05% at the top, respectively (Figs. 4A and 5) with C/N ranging between 9.8 and 8.1. $\delta^{13}C$ reaches high values of −24.8‰ at ca. 390 cm MSL, one of the higher $\delta^{13}C$ values of the entire sedimentary succession (Fig. 5). Phosphates decrease upwards from 1250 to 1175 mg kg^{-1}, reaching a low concentration value of 590 mg kg^{-1} at ca. 390 cm MSL and P decrease from ca. 500 mg kg^{-1} to 250 mg kg^{-1} at ca. 370 cm MSL, slightly increasing upwards to ca. 350 mg kg^{-1} (Fig. 6; Table 3).

Sub-unit 6B (between 410 and 460 cm MSL) is only 50 cm thick, but it is characterized by increases in the OM (increasing from 3.1% to 5.6%), C_{org} (minimum values of 0.6% at the base, reaching 1.5% at 440 cm MSL), N (increasing from 0.07 at the base to 0.14 at the top), PO_4^{-3} (increasing upwards from ca. 830 to ca. 1350 mg kg^{-1}) and P (also increasing upwards from concentration of 340–460 mg kg^{-1}) contents. By opposition, MS values decrease to minimum values of ca. 30 × 10^{-5}. $\delta^{13}C$ is in general lower than in Sub-unit 6A (Figs. 4A, 5 and 6).

Sub-unit 6C corresponds to the top 150 cm of the core, deposited during the last 50 years. It is composed by slightly sandy mud, with CF contents always higher than 10%. Among the sediment, a plastic fragment of polyethylene of recovered at ca. 580 cm MSL (Fig. 4B). It is characterized by a new increase in the MS values with a maximum peak of 61 × 10^{-5} at the base of the Sub-unit (Fig. 4A). The OM contents decrease, C_{org} has lower values but with two peaks at 520–530 and 600–610 cm MSL exceeding the 1% (Fig. 5). Nitrogen increase from 0.05% at the base to 0.18% at the very top, but two values of 0.12% were measured between 520 and 530 cm MSL (Fig. 5). Phosphates and P have similar behaviours varying between 624 and 1731 mg kg^{-1} and 280 and 480 mg kg^{-1}, respectively (Fig. 7) with the higher values at the very top of the core.

5. Discussion

5.1. Source of materials in the upstream reaches of the Sado estuary during the Mid-Late Holocene

The sandy gravel sediment from Unit 0 lacks in organic materials and its source can only be achieved based on the characterization of clasts. The presence of angular centimetric clasts containing essentially quartz and quartzite with the presence of greywacke, granite, shale and sandstone point to the proximity of the source area and to the important influence that Rio Xarrama, that crosses rocks from the South Portuguese Zone (Pulo do Lobo formation) and from Ossa-Morena Zone (granites, diorites and gabbros; Fig. 2B), has concerning the supply of material to the Sado, at least before 4400 cal BP (Fig. 8A).

C/N, $\delta^{13}C$ and $\delta^{15}N$ data are frequently used as proxies for the source of the organic matter and for the reconstruction of paleo sea-level curves (e.g. Meyers, 1994, 1997; Wilson et al., 2005a, 2005b; Lamb et al., 2006; Castro et al., 2010; Khan et al., 2015) since, even after early degradation processes, paleoenvironmental and source information remains preserved in the molecular and isotopic composition of the organic materials (e.g. Meyers, 1994). Particular attention should be given to $\delta^{15}N$ since its degradation could lead to either depletion or enrichment of ^{15}N (e.g. Meyers, 1997) and it can result from the introduction of terrestrial derived inorganic N. However, in Laxique, the correlation between OM and C_{org} and N is positive and very significant, with R^2 values of 0.96 and 0.95, respectively, reflecting mainly an organic source for the materials in spite of dependent on sediment particle size (e.g. Rumolo et al., 2011; Gao et al., 2012). Similarly, the correlation between C_{org} and N is positive and very significant for all the defined Units reflecting the same source of both organic components within each Unit (Fig. 9A). $\delta^{13}C$ values vary between −26.8 and −25.6‰, C/N between 7.9 and 10.8 (Fig. 5) and $\delta^{15}N$ between 4.6 and 7.4‰ in Units 1 to 5 (Fig. 6; Table 3) pointing to materials originating mainly in terrestrial and freshwater environments (e.g. Lamb et al., 2006; Castro et al., 2010, Fig. 9B and C).

Comparing the Laxique isotopic values and C/N ratio with the data obtained from Arapouco and ALC-S (Fig. 9), they are quite similar to the values determined for the sediments accumulated in the alluvial plain (Arapouco Unit 5) and differ from the values determined for the ancient (Arapouco Unit 2 to 4) and current intertidal areas (Arapouco superficial sample and ALC-S), confirming the strong influence of freshwater and terrestrial organic materials reaching Laxique in the Late Middle and early Late Holocene.

In Unit 5 $\delta^{13}C$ values are lower than in Units 1 to 4 (Fig. 5) and seem to reflect an increase in the contribution of organic matter from terrestrial plants and freshwater phytoplankton (Fig. 9B and C). In Unit 6 the isotopic values and C/N ratio deviate from the values determined for the Units below (Units 1 to 5) showing higher $\delta^{13}C$ and $\delta^{15}N$ values and lower C/N ratios that most probably are related to the anthropic manipulation of the area, by the addition of manure and fertilizers in agriculture and the discharge of wastewaters into rivers and coastal areas (see discussion 5.6 below).

Despite relative homogeneity in C and N values, changes in the other analysed proxies, including nutrients, suggest modifications in the environmental conditions, particularly between Units 1 and 4. In Laxique, the contents of nutrients are not related to texture ($R^2 < 0.2$), OM ($R^2 < 0.05$) or C_{org} ($R^2 < 0.1$). The chemistry of nutrients in aquatic sediments is complex and thus, good correlations with other sediment components are not always found. For instance, the lack of correlation between the distribution of phosphorus and the organic matter content could be related to the low C_{org} content, to the complex nature of the organic matter itself, to the predominance of inorganic-P forms and to the intricate relationship among the different sediment components (coating formation, particle cementation, competition for adsorption sites, among others), as observed by Pardo et al. (2003). In Laxique sediments, P, in phosphate (PO_4^{-3}) and total forms (P_t) may reflect the importance of minerals inherited from the setting lithologies. The geology of the drainage area of the Sado river, characterized by a high diversity of sedimentary rocks with carbonate nature (sandstones, conglomerates, limestones and marls) and a high diversity of igneous, metamorphic and metavolcanic rocks, a few of them bearing massive sulphide pollymetalic deposits, may represent a greater source of P, from mineralogical forms as apatite (Ca–P), to phosphate anions fixed/adsorbed in/on sheet silicates and Fe-, Al-oxi-hydroxides (e.g. Zhang and Kovar, 2000; Slomp, 2011; Koziorowska et al., 2018), common weathering products of the aforementioned lithologies (Fonseca et al., 2011). Given this, in-depth changes in P and PO_4^{-3} will point essentially

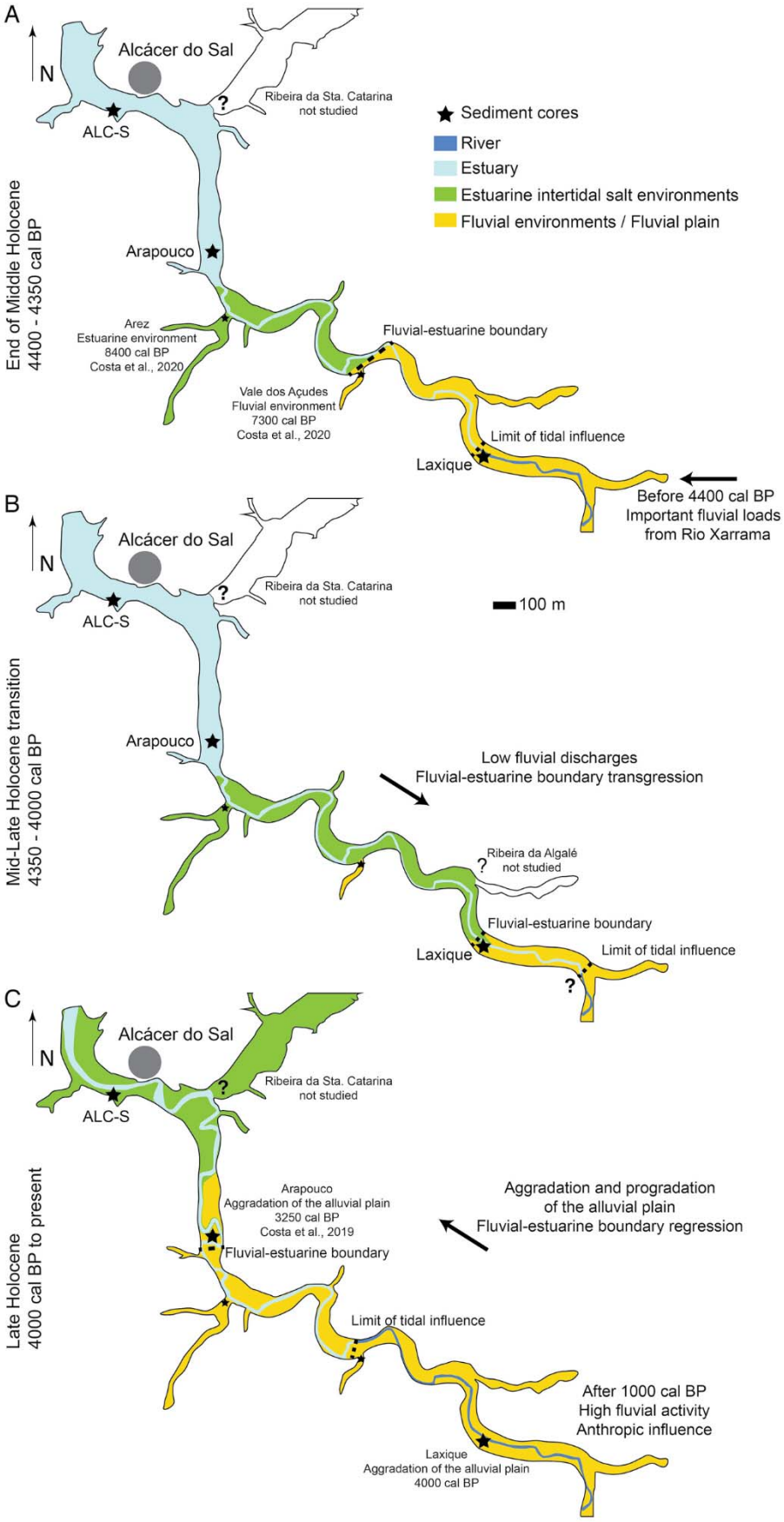

Fig. 8. Schematic model proposed for the paleoenvironmental evolution and fluvial-estuarine boundary changes of the Sado estuary since the end of the Middle Holocene. A – Units 0 and 1; B – Units 2 to 4; C – Units 5 and 6.

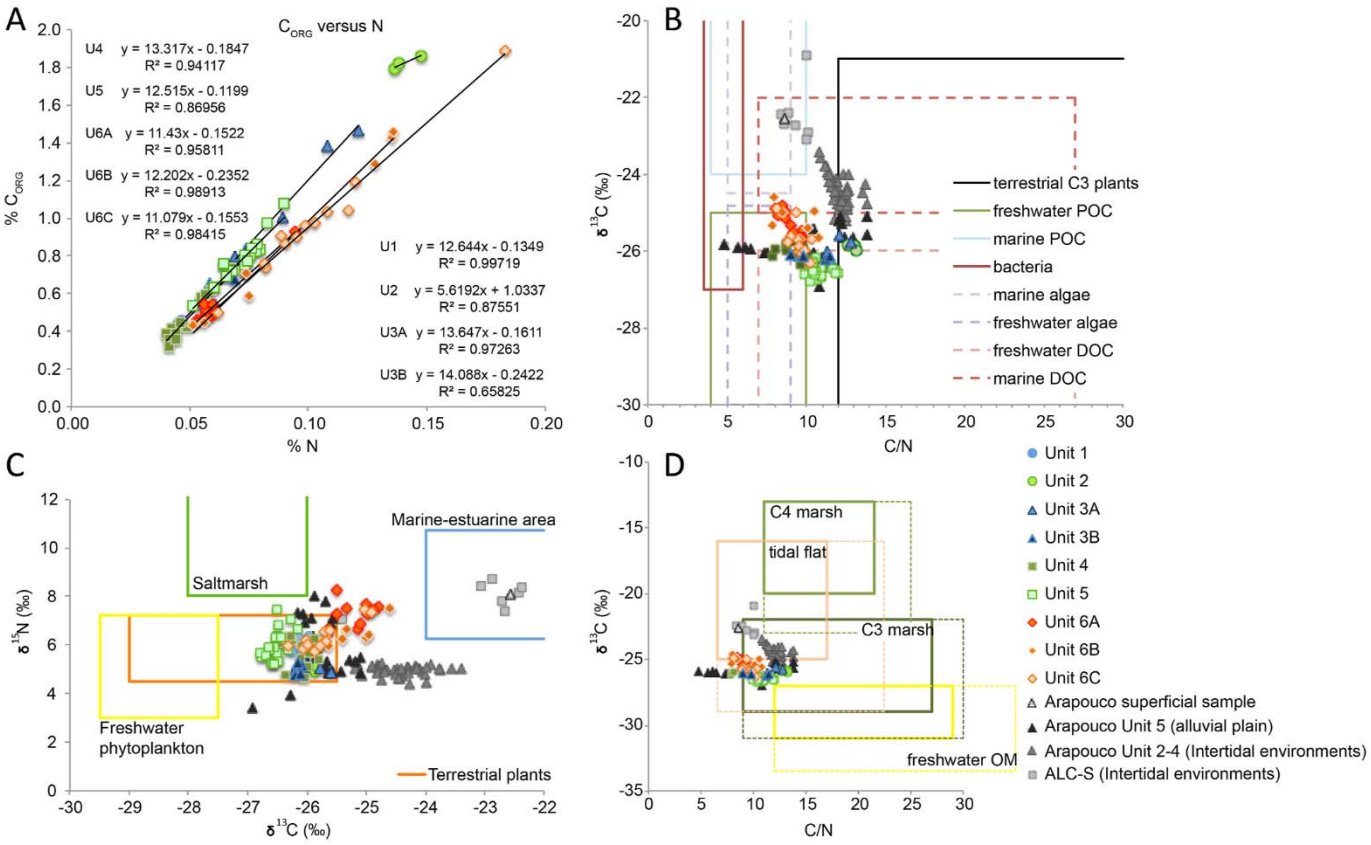

Fig. 9. A. Correlation between % Corg and % N; B. Source of organic materials according to Lamb et al. (2006); C. Source of organic materials according Castro et al. (2010); D. Source of organic materials according to Khan et al. (2015). Dashed lines in Khan et al.'s chart indicates shift in values from modern to Mid-Early Holocene organic compounds due to early degradation processes.

to high/lower river flows and sediment load to the estuary. Other nutrients and also, at a lesser extent, P and PO_4^{-3} content changes in the sedimentary column are most likely dependent on nutrient biogeochemical processes.

5.2. Environmental characterization at the end of Middle Holocene at Laxique

Unit 1, accumulated between ca. 4400 and 4350 cal BP, is coarser, with Fe-oxides precipitations in some quartz grain surfaces and Fe-minerals (Fig. 4A), P and PO_4^{-3} with low concentration, such as organic materials (Figs. 5 and 6) pointing to higher fluvial influence and

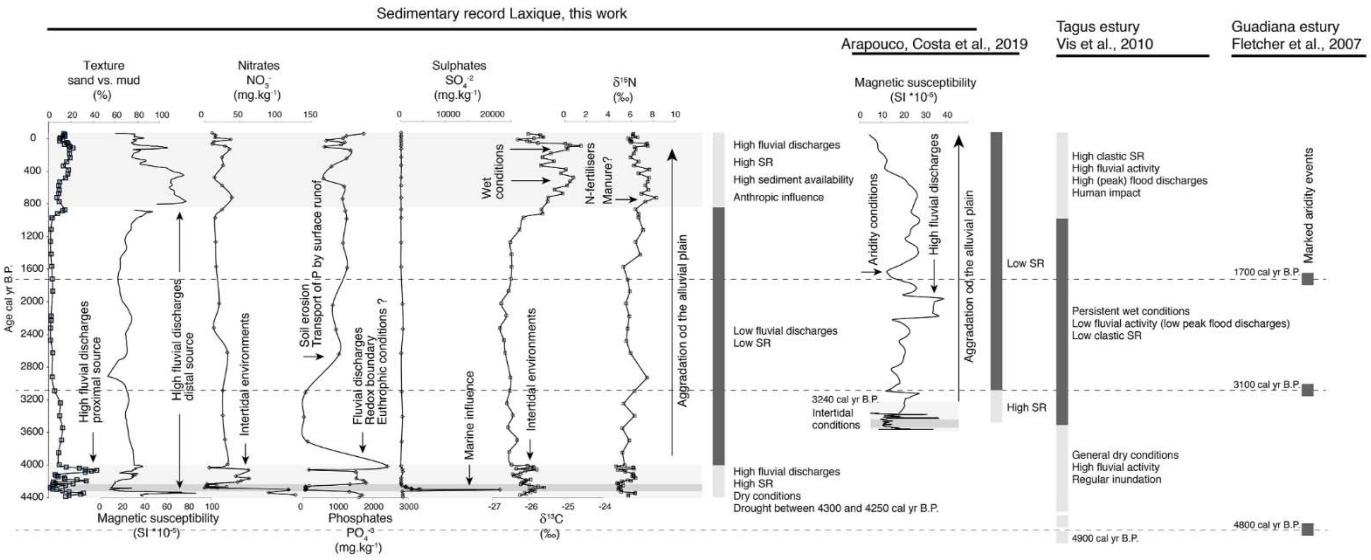

Fig. 10. Summary of environmental changes at Laxique and Arapouco (Costa et al., 2019) in the Sado, the Tagus (Vis et al., 2010) and the Guadiana (Fletcher et al., 2007) valleys. Analysed proxies plotted against age cal BP.

relative higher energetic conditions. Magnetic particles, sourced from the Iberian Pyrite Belt (Fig. 2A), are also transported and accumulated in the area (Fig. 4). The deposition of Unit 1 can result from high precipitation events, in a prevailing drier climate (e.g. Fletcher et al., 2007) that increased river transport competence. Accordingly, the fluvial and terrestrial particulate organic carbon combined adds up to more than 80%, according to the values determined by the equations used by Alonso-Hernandez et al. (2007) (Fig. 5), with ca. 60% POC derived from freshwater sources. High river discharges during high precipitation events are typical of Mediterranean rivers and the occurrence of such conditions during the deposition of Unit 1 allows to characterize the Sado as a Mediterranean river, with a strong Mediterranean character, at least, since the end of the Middle Holocene. Indeed, western Mediterranean Late Holocene is characterized by prevailing drier climatic conditions since ca. 5000-4000 cal BP (Fletcher et al., 2007, 2013; Carrión et al., 2010; Chabaud et al., 2014; Gomes et al., 2020) with peaks of high fluvial activity that promote regular to sporadic inundation of distal estuarine areas in South Iberia (Vis et al., 2010, Fig. 10). The availability of sediment can also result from vegetation retreat due to the establishment of drier climatic conditions (e.g. Fletcher et al., 2007, 2013; Carrión et al., 2010; Chabaud et al., 2014; Gomes et al., 2020).

In Unit 2, deposited between 4350 and 4300 cal BP, coarse materials decrease to the top such as the magnetic materials (Fig. 4A) while organic compounds increase, reaching to maximum values in OM, C_{org} (Fig. 5) and N (Fig. 6), reflecting a low energy environment with limited fluvial inputs. Organic matter sourced in freshwater organic materials seem to have a higher abundance in the total organic matter content, slightly decreasing the organic matter with terrestrial origin (Figs. 5 and 9). The presence of gypsum in Unit 2 is also indicative of dry conditions.

In both Units 1 and 2 diatoms are absent, but bioturbation and macro-plant remains were identified. This upward fine succession accumulated between −195 and −130 cm (Units 1 and 2, total 65 cm thickness) may result from deposition in a tidal flat (sandflat to mudflat)/C3 marsh environment (Fig. 9C; Khan et al., 2015), in the transition zone between the fluvial-estuarine boundary and the limit of tidal influence with very low to absent salinity contents, receiving essentially organic material from terrestrial and freshwater sources, similar to the conditions currently prevailing upstream Arapouco (Figs. 1 and 8A).

Assuming a mean sea-level rise rate of 0.31 mm yr^{-1} (Costas et al., 2016), a MSL placed at −140 to −130 cm below the present-day MSL during the interval between 4400 and 4300 cal BP and considering tidal characteristics similar to the present, the development of tidal flat areas are expected. Presently, the Sado intertidal platforms develop between −1.8 and 2 m MSL (Moreira, 1992).

In addition both Units present the highest contents of NO_3^- of the sedimentary succession, and high contents of PO_4^{-3} and P (Fig. 7). The high concentration of NO_3^- can result from high rates of atmospheric N fixation by aquatic organisms. In upper estuarine shallow environments, turbidity conditions and light limitations limit the uptake of nitrate by benthic nitrifying communities. In such conditions NO_3^- can be buried in sediments under the presence of oxidizing conditions (e.g. Scanes et al., 2017). It can also result from high NO_3^- and NH_4^+ fluvial inputs into the system, followed by high nitrification rates in the estuarine superficial sediments and rapid burial and storage due to high SR. In coastal shallow waters nitrification is enhanced, for instance, by the input of organic materials (e.g. Henriksen and Kemp, 1988).

As mentioned above, the high concentration of P and PO_4^{-3} can derive from higher fluvial activity (Fonseca et al., 2011).

5.3. Maximum extension of the estuarine (saline) area at the Middle to Late Holocene transition

Unit 3A, accumulated between 4300 and 4250 cal BP, is characterized by high contents of SO_4^{-2}, by the presence of gypsum at the base and by the presence of diatoms (Figs. 4B and 7), while NO_3^-, PO_4^{-3} and P decrease to minimum values (Fig. 6) pointing to the flooding of marine waters and low fluvial activity. The diatoms in this Sub-unit indicate initial tidal conditions, moving in the uppermost part to a subtidal environment characterized by the dominance of the marine semi planktonic *Cymatosira belgica* which outnumbers benthic/epiphytic diatoms.

Nowadays the fluvial-estuarine boundary is placed near Arapouco (Figs. 1B and 8C; Bettencourt and Ramos, 2003), but only influences the present-day Sado channel, a narrow channel incised in the alluvial sediments that are essentially fed by the fluvial network during flooding episodes (Costa et al., 2019). Estuarine conditions were present at Arapouco until ca. 3240 cal BP, being the fluvial-estuarine boundary by that time located at upstream reaches of the Sado still unknown (Costa et al., 2019).

According to paleocological and paleoenvironmental data and taking into consideration the depth of the Unit (−130 to −90 MSL) and contemporary MSL (ca. −130 cm MSL assuming a MSL rise rate of 0.31 mm yr^{-1}; Costas et al., 2016), at the time of deposition of Unit 3A the fluvial-estuarine boundary was located near Laxique, allowing for the occasional flooding of the area by marine waters (Fig. 8B). Even under marine influence, organic source indicators (C_{org}, N_{Tot}, $\delta^{13}C$, $\delta^{15}N$) point to the prevalence of terrestrial and freshwater organic materials, being the incorporation of marine organic matter recorded by a slightly increase in the $\delta^{13}C$ values (Figs. 5 and 9), reflecting the proximity of the freshwater and terrestrial organic sources to the study area and indicating the very upstream limit of the estuarine area at the transition to the Late Holocene.

Similarly to what was described for other portuguese (Azevêdo et al., 2010; Baptista et al., 2010) and worldwide estuaries (Liu et al., 2007; Shaha and Cho, 2016; Robins et al., 2018; Ospino et al., 2018), low river discharges enhance marine water intrusion, certainly promoting changes in the environmental conditions. Similar to what was interpreted for Arapouco (Costa et al., 2019), the influence of marine waters at upstream areas of the Sado could have resulted from low river discharges due to low precipitation periods. At Laxique, low fluvial discharge during the deposition of Unit 3A is attested by the low values of MS and by the prevalence of muddy sediments. Sado has a Mediterranean flow regime with high seasonal variable fluvial discharges and occasional flow peaks. Variable flow river systems are less effective in controlling estuarine stability (Azevêdo et al., 2010), certainly allowing for fluctuations on the fluvial-estuarine boundary. In addition, positive of sea-level rise rate oscillations promoted by regional climatic factors (e.g. Church et al., 2013) and enhanced storminess periods, can also affect the position of the fluvial-estuarine boundary. Indeed, in the curve draw by Costas et al. (2016) that modulates the MSL rise for the last 6500 years in the Sado estuary, small positive oscillations of MSL were identified, particularly ca. 4000 years ago. These oscillations were not further studied due to method resolution. However, most probably, small MSL oscillations under a prevailing drier climate (e.g. Fletcher et al., 2007; Chabaud et al., 2014; Gomes et al., 2020) and low fluvial activity will contribute to enlargement of the estuarine area and to the retreat of the fluvial-estuarine boundary. It is also worth noting that a shoreline retreat was identified in the Tróia spit at ca. 4000 years ago (Costas et al., 2015). A similar pattern, with increased marine influence and retreat of the fluvial-estuarine boundary seemed to have occurred at Arapouco, despite later, between 3400 and 3300 cal BP (Costa et al., 2019), derived from similar conditions, evidencing recurrent fluctuations of the fluvial-estuarine boundary mostly due to climate factors and, at a lesser extent, MSL oscillations. Fluctuations on the MSL rise rate have not yet been identified in the curves draw for the Tagus estuary. Notwithstanding, the record of changes in the MSL rise rate and the influence of such oscillations in the environmental conditions of both estuaries can also be dependent on these two river hydrological parameters that differ severely, at least considering their natural mean annual flows.

Unit 3B, accumulated between 4250 and 4200 cal BP, is characterized by new fluvial inputs reflected by the increase in the sand content (Fig. 4A). Nitrate, PO_4^{-3} and P increase while SO_4^{-2} decrease pointing to the regression of the fluvial-estuarine boundary and to the establishment of more fluvial conditions. However, diatom assemblages indicate to some extent still the influence of marine water (Figs. 4 and 7). Diatom assemblages are made by common benthic and widespread species in intertidal zones of estuaries and marine coasts worldwide. Assemblage is dominated by large mobile epipelic species characteristic of mudflats environments.

Unit 4, accumulated between 4200 and 4000 cal BP, marks the transition to the upper intertidal environments. It is characterized by episodes of fluvial sediment loads reflected by the increase of sandy sediments (Fig. 5) and the slightly increase in MS values. At Arapouco (Costa et al., 2019) magnetic particles/elements were associated with the fine particles. However, the presence of FeO minerals and quartz grains with Fe coating will likely be influencing the magnetic response of the sediments at Laxique. Arapouco locates ca. 15 km downstream Laxique. According to our results, under high stream discharges coarse sediments accumulate at the upstream reaches of the estuarine area while finer sediments with magnetic particles are transported and accumulated more downstream. Nitrate, PO_4^{-3}, P and SO_4^{-2} contents are similar to Sub-unit 3B decreasing in the top of the Unit (Fig. 6), probably in response to the increase of coarse particles. The sharp variations of PO_4^{-3} at the transition to Unit 5 is most probably reflecting the influence of biogeochemical changes (ancient redox boundaries) in the sediment profile than environmental changes once PO_4^{-3} tend to be retained in the sediment in the presence of oxidizing conditions (e.g. Scanes et al., 2017). The presence of shallow and sharp redox potential boundary in the sediment can point to high organic matter supply and to low bioturbation, indicating eutrophic conditions at ca. 4000 cal BP.

Unit 4 is a threshold considering the marine influence at Laxique. From 4000 cal BP onwards, sedimentation occurs essentially under fluvial conditions with sedimentation contributing to the aggradation of the alluvial plain. Since 4000 years ago the progradation rate of the Tróia sand spit increased and the barrier grew north (Costas et al., 2015) certainly reducing the water exchange between the sea and the river and allowing for the progradation of fluvial environments.

5.4. Environmental characterization at the Middle to Late Holocene transition

Similarly to Units 1 and 2, Units 3 and 4 accumulate at mean high SR of 0.75 cm y^{-1} (Fig. 3), higher than the mean sea-level rise rate determined for the Late Holocene (ca. 0.31 mm yr^{-1}; Costas et al., 2016). According to sediment depths (−130 to 88 cm MSL) and the projected depth for the MSL at that time (−130 to −120 cm MSL) the environmental conditions changed from a tidal flat to an upper intertidal area offering conditions for the development of saltmarshes. However the presence of a saltmarsh at the beginning of the Late Holocene at Laxique is difficult to access. $\delta^{13}C$ determined for Units 3 and 4 are quite similar with the values measured for the Units 1 and 2 (below), reflecting essentially organic materials sourced in terrestrial and freshwater environments. The Sado channel margins at Alcácer do Sal and Arapouco, that represent the present-day fluvial-estuarine boundary and where low salinity values of 0–0.5‰ are present due mostly to tidal processes (e.g. Ferreira et al., 2003), are essentially colonized by *Phragmites australis* (C3 photosynthetis pathway) (Moreira, 2016), an autochthonous cosmopolitan species that tolerates a high variety of environments. Freshwater marshes are not described at present in the Sado freshwater wetlands, but could have existed in the past as described between 6700 and 5800 cal yr BP in the Muge stream, a Tagus tributary (van der Schriek et al., 2007). At present, Sado riverine margins are highly anthropized, frequently used as agricultural fields, mostly rice crops (Fig. 1C) and most possible inhibit the development of natural freshwater environments. Organic chemical data produced from superficial and deeper sediments collected in Arapouco (Costa et al., 2019) and Alcácer do Sal (superficial sediments) present higher C/N, $\delta^{13}C$ and $\delta^{15}N$ values than the values determined for Units 1 to 4 (Figs. 5, 6 and 9). The differences in these values can result from i) post-depositional processes such as bioturbation, diagenesis or microbial degradation that are known to affect sediment chemical signals through time, with most expression at a scale of thousands of years, i.e. Early-Mid Holocene records (e.g. Khan et al., 2015); and ii) a higher contribution of local C3 (saltmarsh) plants and terrestrial/freshwater organic materials (lower $\delta^{13}C$, $\delta^{15}N$ and N) in relation to marine organic matter (higher $\delta^{13}C$, $\delta^{15}N$ and N). Considering the present-day similar environmental characteristics for intertidal areas of Alcácer do Sal and Arapouco that were taken as analogues for Laxique , the difference in the values do not support the existence of a saltmarsh, and most probably result from an intertidal area with strong fluvial influence, despite the influence of marine waters, as pointed out by the similarity of values between Laxique Units 3 and 4 and Arapouco alluvial sediments (Unit 5). By opposition, the difference in the values determined between the present-day (ALC-S and Arapouco superficial sediment) and old (Arapouco Unit 2–4) intertidal sediments (Fig. 8) point to changes due to post-depositional processes indicating that such processes should be taking into consideration also for the beginning of the Late Holocene, at least, for mid latitude sites as SW Iberia.

5.5. Sedimentation rates, aggradation and progradation of the alluvial environments

Sedimentation rates are highly dependent on river flows, sediment availability and accommodation space (e.g. Brown, 1997). Sado has a deep incised paleovalley reaching 40 m depth at Alcácer do Sal and ca. 38 m depth at São Bento (Costa et al., 2020) offering accommodation space for the deposition of sediments through the Late Quaternary. The sedimentary pattern and the valley morphology evolution for the Sado during the Early and Middle Holocene are still unknown. Nevertheless, according the sedimentary record from Laxique, the valley still offered conditions, i.e., accommodation space, for the deposition of sediments influenced by marine waters during the Late Holocene, under prevailing low sea-level rise rates (e.g. Costas et al., 2016; García-Artola et al., 2018). Hereupon, sedimentation is mostly dependent on river flows and sediment availability.

Sedimentation rates determined for the three sediment cores collected in the intertidal margin at Alcácer do Sal (ALC-S) and at the alluvial plain at Arapouco and Laxique (Fig. 3) deposited during the Mid-Late Holocene transition and Late Holocene onwards indicate high SR in depth, for sediments accumulating under low subtidal/intertidal conditions until MSL, and lower SR for sediments deposited above MSL corresponding to the aggradation of fluvial materials and building-up the alluvial plain. Considering the higher SR, that exceeds the sea-level rise rate, the available accommodation space silts-up rapidly leading to the aggradation of the alluvial plain (low SR) and to the progradation of the fluvial environments. The aggradation of the alluvial plain initiates at 4000 cal BP at Laxique and took place at 3240 cal BP at Arapouco (Costa et al., 2019, Fig. 8C). According to Moreira (1992) saltmarshes started to develop since, at least, 2700 cal BP at the intertidal margins of the present-day estuary. At Alcácer do Sal the subtidal margins were silted-up between the 13th and 14th centuries, allowing for the development of present-day saltmarshes (Moreira, 2016). At present saltmarshes develop in intertidal environments of the estuary occupying an area of ca. 7.2 km^2 (Moreira, 1992).

Unit 5 accumulated between 4000 and 960 cal BP, corresponds to the aggradation of the alluvial plain at slow SR of 0.06 cm y^{-1}. Sediments represent a fine-up sequence constituted by sandy mud to mud with low MS pointing to low fluvial activity (peak discharges). Similar conditions of low fluvial activity (low peak fluvial discharges) under general wet conditions were described for the Tagus between 3500 and 1000 cal BP (Vis et al., 2010). A marked aridity event was defined for the Guadiana

at 3100 cal BP (Fletcher et al., 2007) (Fig. 10). $\delta^{13}C$ values are low and C/N ratio higher than 10 reflecting the terrestrial/fluvial source of the OM (e.g. Lamb et al., 2006; Khan et al., 2015). Phosphate and P contents increase in Unit 5 (Fig. 7). The transfer of phosphorus to estuaries can be made through surface runoff that mobilizes particulate and dissolved P forms from land. In addition, the erosion of soils in areas with forest retreat greatly increased the contents of P that are transported to rivers and estuaries once most soils highly contribute to retain P (e.g. Slomp, 2011). Palynological evidences from SW Iberia indicate a retreat in the forest cover and progressive expansion of shrublands and heathlands since ca. 5000 cal BP (e.g. Fletcher et al., 2007, 2013; Chabaud et al., 2014; Gomes et al., 2020) that certainly allowed for soil erosion and the transport of sediments by surface runoff to the river (Fig. 10). Evidence of anthropic influence on the landscape was recognized in both the Tagus (ca. 6000 cal BP) and the Guadiana (ca. 5000 cal BP) surrounding areas since the Middle Holocene (Fletcher et al., 2007; Vis et al., 2010).

5.6. Anthropic influence

Unit 6 also corresponds to the aggradation of the alluvial plain accumulated during the last 1000 years, with MSL similar to the present-one. Similarly to the scenario described for the Tagus estuary (Vis et al., 2010), SR increase (Fig. 3) in response to higher sediment availability and higher fluvial (peak discharges) activity (Fig. 10) as reflected by the slightly increase in the sand content and the high MS values (Fig. 4). $\delta^{13}C$ increase reaching values higher than −25‰ particularly in Sub-units 6A and 6B. In pristine estuarine environments higher $\delta^{13}C$ values point to marine influence, with contribution of marine organic materials to the bulk organic matter (Lamb et al., 2006; Khan et al., 2015). However, Unit 6 correspond to the top 3 m of the sedimentary succession, accumulated at depths between 290 and 610 cm above present-say MSL, where the intrusion of marine water is not possible considering present-day local tidal conditions. $\delta^{13}C$ and $\delta^{15}N$ values of plant and soils are known to be affected by the application of manure and mineral fertiliser in crop areas (e.g. Senbayram et al., 2008; Treasure et al., 2016). According to several published works, soils with high contribution of organic N (e.g. manure) present higher $\delta^{15}N$ values than unfertilized soils or mineral-fertilised soils (e.g. Senbayram et al., 2008; Fiorentino et al., 2015). $\delta^{13}C$ values are also affected by the input of N-fertilisers, with soil $\delta^{13}C$ values decreasing with the application of manure (e.g. Bol et al., 2005; Senbayram et al., 2008). Notwithstanding, plant $\delta^{13}C$ values seem not to be affected by manuring increase with the application of mineral-N fertilisers (e.g. Bogaard et al., 2013), but are strongly influenced by environmental conditions, particularly by water availability (e.g. Jenkinson et al., 1995; Senbayram et al., 2008) making isotopic studies relevant considering past environmental conditions (eg. Bogaard et al., 2013; Fiorentino et al., 2015). In dry years (drought), $\delta^{13}C$ tend to be lower and in optimal environmental conditions (water availability) $\delta^{13}C$ is higher (e.g. Senbayram et al., 2008; Bogaard et al., 2013; Fiorentino et al., 2015). In Laxique, both $\delta^{13}C$ and $\delta^{15}N$ present high values (Figs. 5 and 6), pointing to the inclusion of fertilisers in the study area since, at least, ca. 700 cal BP (Fig. 10). Additionally, MS and the sand content increase, pointing to high fluvial activity, and possibly to wetter conditions that contribute to higher $\delta^{13}C$ values in the bulk organic sediment, particularly between ca. 625 and 280 cal BP (Sub-unit 6A) and the last 50 years (Sub-unit 6C; Fig. 10). Records point to rice production in the Sado since, at least, the 18th century, nevertheless, it probably started before (Carmo et al., 2020). At present in the Sado area, rice is produced in continuous flooding conditions, where the soil is maintained waterlogged for several months and N-fertilisers added to soils (e.g. Figueiredo et al., 2014). The continuous flooding of soils and the addition of N can contribute to the high $\delta^{13}C$ values determined at the top core meters. Recent anthropogenic influence (Sub-unit 6C, accumulated during the last 50 years) is also attested by the presence of polyethylene fragments within the sediment (Fig. 4), at ca. 25 cm depth. Polyethylene began to be produced in the late 1930's and 40's, its expansion and usage diversification started at ca. '50s and it's still produced nowadays (e.g. Zalasiewicz et al., 2016).

6. Conclusions

The multiproxy analysis of a 10.5 m sedimentary sequence recovered from the upstream reaches of the Sado revealed to be a source of information concerning paleoenvironmental characterization and fluvial responses to climate variability during the Middle to Late Holocene in a Mediterranean river.

During the Mid-Late Holocene transition the Sado estuary has experienced significant changes in the fluvial-estuarine boundary. The occurrence of marine diatoms at Laxique between 4300 and 4200 cal BP locates the fluvial-estuarine boundary ca. 65 km upstream the present-day estuary inlet and ca. 15 km upstream the present-day boundary, at Arapouco. Even during periods with higher marine influence, the organic matters at the fluvial-estuarine boundary is transported by the fluvial network and mostly sourced in freshwater and terrestrial environments, similar to present-day conditions where low to very low salinity contents are attested.

Prevalent Late Holocene dry climatic conditions in South Iberia, is also attested in Laxique by the presence of gypsum precipitation in depth. Consequent general retreat of vegetation, low river discharges and, at a lesser extent, oscillations of MSL, are the main responsible for the fluctuations of the fluvial-estuarine boundary location.

The aggradation and progradation of the alluvial plain occurred since ca. 4000 cal BP at Laxique. As typical of Mediterranean rivers, precipitation and consequent fluvial activity, vegetation retreat, sediment availability and loss of accumulation space led to the downstream migration of the fluvial-estuarine boundary, the aggradation and the progradation of the alluvial plain and the abrupt changes in the sedimentation rates.

The fluvial activity and the anthropic influence increase during the last 1000 years, as also attested for the Tagus estuary.

Author contributions

All authors have made substantial contributions to this submission. Ana Maria Costa, Maria da Conceição Freitas, Mariana Diniz and Pablo Arias conceived the study. Ana Maria Costa, Manel Leira, Rita Fonseca and João Duarte made laboratory analysis. Ana Maria Costa, Maria da Conceição Freitas, Manel Leira and Rita Fonseca wrote the manuscript. All authors commented and contributed to improve the manuscript.

Data availability

The data collected during the current study are available from the corresponding author on reasonable request.

Declaration of competing interest

The authors declare that they have no known competing financial interests or personal relationships that could have appeared to influence the work reported in this paper.

Acknowledgements

The authors would like to acknowledge to Ana Filipa Fernandes and Vera Lopes who helped in laboratory sample analyses. Acknowledgment also goes to HERCULES laboratory for μ-FTIR analyses.

Funding: This work was done with-in the PhD grant funded by FCT (SFRH/BD/110270/2015) attributed to Ana Maria Costa between 2016 and 2019 and took advantage of financial support from the projects CoChange (HAR 2014-51830-P), SimTIC (HAR 2017-82557-P) financed by the Spanish Ministry of Science and Innovation, Back to Sado (PTDC/HIS-ARQ/121592/2010) and CLIMARES (PTDC/CTA-GEO/28412/

2017) funded by FCT. The authors would also like to acknowledge the support of the Instituto Dom Luiz - IDL (UIDB/GEO/50019/2020)

References

Alonso-Hernandez, C.M., Garcia-Moya, A., Tolosa, I., Diaz-Asencio, M., Corcho-Alvarado, J.A., Morera-Gomez, Y., Fanelli, E., 2007. Tracing organic matter sources in a tropical lagoon of the Caribbean Sea. Continent. Shelf Res. 148, 53–63. https://doi.org/10.1016/j.csr.2017.08.001.

Andrade, C., Freitas, M.C., Brito, P., Amorim, A., Barata, A., Cabaça, G., Santos, F.D., Miranda, P., Coord, 2006. Estudo de caso da região do Sado, zonas costeiras. Alterações Climáticas em Portugal Cenários, Impactos e Medidas de Adaptação, Projecto SIAM II, pp. 423–436. Lisboa, Gradiva.

Anthony, E.J., Marriner, N., Morhange, C., 2014. Human influence and the changing geomorphology of Mediterranean deltas and coasts over the last 6000 years: from progradation to destruction phase? Earth Sci. Rev. 139, 336–361. https://doi.org/10.1016/j.earscirev.2014.10.003.

Antunes, M.T., 1983. Notícia explicativa da Folha 39-C Alcácer do Sal, Carta Geológica de Portugal 1:50000. Serviços Geológicos de Portugal, Lisboa.

Antunes, M., Pais, J., 1991. *Carta Geológica de Portugal* 1:50000 Folha 39-C Alcácer do Sal. Serviços Geológicos de Portugal. Direcção Geral de Geologia e Minas.

Antunes, M., Pais, J., Gonçalves, F., Oliveira, J., Peleja, A.F., Barroso, J.P., Romão, J.A., Lopes, J.C., Casimiro, J., 1991. *Carta Geológica de Portugal* 1:50000 Folha 39-D Torrão. Serviços Geológicos de Portugal. Direcção Geral de Geologia e Minas.

Azevêdo, I.C., Bordalo, A.A., Duarte, P.M., 2010. Influence of river discharge patterns on the hydrodynamics and potential contaminant dispersion in the Douro estuary (Portugal). Water Res. 44, 3133–3146. https://doi.org/10.1016/j.watres.2010.03.011.

Baptista, J., Martinho, F., Dolbeth, M., Viegas, I., Cabral, H., Pardal, M., 2010. Effects of freshwater flow on the fish assemblage of the Mondego estuary (Portugal): comparison between drought and non-drought years. Mar. Freshw. Res. 61, 490–501. https://doi.org/10.1071/MF09174.

Benito, G., Sopeña, A., Sánchez-Moya, Y., Machado, M.J., Pérez-González, A., 2003. Palaeoflood record of the Tagus river (Central Spain) during the late Pleistocene and Holocene. Quat. Sci. Rev. 22, 1737–1756. https://doi.org/10.1016/S0277-3791(03)00133-1.

Benito, G., Macklin, M.G., Zielhofer, C., Jones, A.F., Machado, M.J., 2015. Holocene flooding and climate change in the Mediterranean. Catena 130, 13–33. https://doi.org/10.1016/j.catena.2014.11.014.

Bettencourt, A., Ramos, L. (Eds.), 2003. *Estuários Portugueses*. Lisboa: Direcção dos Serviços de Planeamento, Instituto da Água, Ministério das Cidades, Ordenamento do Território e Ambiente.

Biguino, B., Sousa, F., Brito, A.C., 2021. Variability of currents and water column structure in a temperate estuarine system (Sado estuary, Portugal). Water 13, 187. https://doi.org/10.3390/w13020187.

Blaauw, M., 2010. Methods and code for 'classical' age-modelling of radiocarbon sequences. Quat. Geochronol. 5 (5), 512–518. https://doi.org/10.1016/j.quageo.2010.01.002.

Blott, S., 2000. GRADISTAT Version 4.0. A Grain Size Distribution and Statistics Package for the Analysis of Unconsolidated Sediments by Sieving or Laser Granulometer.

Bol, R., Eriksen, J., Smith, P., Garnett, M.H., Coleman, K., Christensen, B.T., 2005. The natural abundance of 13C, 15N, 34S and 14 C in archived (1923-2000) plant and soil samples from the Askov long-term experiments on animal manure and mineral fertilizer. Rapid Commun. Mass Spectrom. 19 (22), 3216–3226. https://doi.org/10.1002/rcm.2156.

Bogaard, A., Fraser, R., Heaton, T.H.E., Wallace, M., Vaiglova, P., Charles, M., Jones, G., Evershed, R.P., Styring, A.K., Andersen, N.H., Arbogast, R.-M., Bartosiewicz, L., Gardeisen, A., Kanstrup, M., Maier, U., Marinova, E., Ninov, L., Shäfer, M., Stephan, E., 2013. Crop manuring and intensive land management by Europe's first farmers. Proc. Natl. Acad. Sci. U. S. A. 110 (31), 12589–12594. https://doi.org/10.1073/pnas.13059181110.

Brito, P., 2009. Impactos da elevação do nível médio do mar em ambientes costeiros: o caso do estuário do Sado. PhD thesis. Departamento de Geologia da Faculdade de Ciências, Universidade de Lisboa, Portugal.

Brown, A.G., 1997. Alluvial Geoarchaeology. Floodplain Archaeology and Environmental Change. Cambridge Manuals in Archaeology.

Camacho, S., Boski, T., Moura, D., Scott, D., Connor, S., Pereira, L., 2016. Paleoenvironmental evolution of the Guadiana Estuary, Portugal, during the Holocene: a modern foraminifera analog approach. Holocene 27 (2), 197–235. https://doi.org/10.1177/0959683616658526.

Carmo, M., Sousa, J., Varela, P., Ventura, R., Bivar, M., 2020. African knowledge transfer in Early Modern Portugal: Enslaved people and rice cultivation in Tagus and Sado rivers. Diacronie. Studi di Storia Contemporanea: "*Can the subaltern speak" attraverso l'ambiente*?, 44 http://www.studistorici.com/2020/12/29/sousa-bivar-carmo-varela-ventura_numero_44/.

Carrión, J.S., Fernández, S., González-Sampériz, P., Gil-Romera, G., Badal, E., Carrión-Marco, Y., López-Merino, L., López-Sáez, J.A., Fierro, E., Burjachs, F., 2010. Expected trends and surprises in the lateglacial and Holocene vegetation history of the iberian Peninsula and balearic islands. Rev. Palaeobot. Palynol. 162, 458–475. https://doi.org/10.1016/j.revpalbo.2009.12.007.

Cartelle, V., García-Gil, S., 2019. From a river valley to a ria: evolution of an incised valley (Ría de Ferrol, north-west Spain) since the Last Glacial Maximum. Sedimentology 66 (5), 1930–1966. https://doi.org/10.1111/sed.12565.

Castro, D.F., Rossetti, D.F., Pessenda, L.C.R., 2010. Facies, $\delta^{13}C$, $\delta^{15}N$ and C/N analyses in a late Quaternary compound estuarine fill, northern Brazil and relation to sea level. Mar. Geol. 274, 135–150. https://doi.org/10.1016/j.margeo.2010.03.011.

Chabaud, L., Sánchez Goñi, M.F., Desprat, S., Rossignol, L., 2014. Land–sea climatic variability in the eastern North Atlantic subtropical region over the last 14,200 years: atmospheric and oceanic processes at different timescales. Holocene 24, 787–797. https://doi.org/10.1177/0959683614530439.

Church, J.A., Clark, P.U., Cazenave, A., Gregory, J.M., Jevrejeva, S., Levermann, M.A., Merrifield, M.A., Milne, G.A., Nerem, R.S., Nunn, P.D., Payne, A.J., Pfeffer, W.T., Stammer, D., Unnikrishnan, A.S., 2013. sea level change. In: Stocker, T.F., Qin, D., Plattner, G.-K., Tignor, M., Allen, S.K., Boschung, J., Nauels, A., Xia, Y., Bex, V., Midgley, P.M. (Eds.), Climate Change 2013: the Physical Science Basis. Contribution of Working Group I to the Fifth Assessment Report of the Intergovernmental Panel on Climate Change. Cambridge University Press, United Kingdom and New York, USA, pp. 1137–1216.

Cid, N., Bonada, N., Carlson, S.M., Grantham, T.E., Gasith, A., Resh, V.H., 2017. High variability is a defining component of mediterranean-climate rivers and their biota. Water 9 (1), 52. https://doi.org/10.3390/w9010052.

Costa, Ana Maria, Freitas, Maria, Leira, Manel, 2021. Sedimentology and organic content and chemistry data from the Sado estuary. https://doi.org/10.17632/wb73343r4v.1. Mendeley Data, V1.

Costa, A.M., Freitas, M.C., Leira, M., Costas, S., Costa, P.J.M., Andrade, C., Bao, R., Duarte, J., Rodrigues, A., Cachão, M., Araújo, A.C., Diniz, M., Arias, P., 2019. The role of climate, marine influence and sedimentation rates in Late Holocene estuarine evolution (SW Portugal). Holocene 29, 622–632. https://doi.org/10.1177/0959683618824768.

Costa, A.M., Freitas, M.C., Mota, R., Leira, M., Andrade, C., Pimentel, N., Araújo, A.C., Bao, R., Diniz, M., Arias, P., 2020. Sado palaeovalley configuration: implications for the Mesolithic settlement during the Holocene sea-level rise. In: Roque, A., Brito, C., Veracini, C. (Eds.), People, Nature and Environments: Learning to Live Together. Part 4 - Landscape and Heritage, Chapter Thirteen. Cambridge Scholars Publishing, pp. 176–194.

Costas, S., Ferreira, O., Plomaritis, T.A., Leorri, E., 2016. Coastal barrier stratigraphy for Holocene high-resolution sea-level reconstruction. Sci. Rep. 6, 38726.

Costas, S., Rebêlo, L., Brito, P., Fitzgerald, D., 2015. The joint history of Tróia península and Sado ebb-delta. In: Randazzo, G., Jackson, D.W.T., Cooper, J.A.G. (Eds.), Sand and Gravel Spit. Spinger, pp. 79–102.

Dabrio, C.J., Zazo, C., Goy, J.L., Sierro, F.J., Borja, F., Lario, J., González, J.A., Flores, J. A., 2000. Depositional history of estuarine infill during the last postglacial transgression (Gulf of Caidz, Southern Spain). Mar. Geol. 162, 381–404. https://doi.org/10.1016/S0025-3227(99)00069-9.

Degeai, J.-P., Bertoncello, F., Vacchi, M., Augustin, L., de Moya, A., Devillers, B., 2020. A new interpolation method to measure delta evolution and sediment flux: application to the late Holocene coastal plain of the Argens River in the western Mediterranean. Mar. Geol. 424, 106159. https://doi.org/10.1016/j.margeo.2020.106159.

ENGIVIA, Consultores de Engenharia Lda (n.d.), A2, auto-estrada do sul. Sublanço alcácer do sal/grândola norte, PE1-terraplanagens, Parte 1.4-Geologia e geotecnia, Volume V.

Flemming, B., 2000. A revised textural classification of gravel-free muddy sediments on the basis of ternary diagrams. Continent. Shelf Res. 20, 1125–1137. https://doi.org/10.1016/S0278-4343(00)00015-7.

Ferreira, J.G., Simas, T., Nobre, A., Silva, M.C., Shifferegger, K., Lencart, S.J., 2003. Identification of areas and vulnerable zones in transitional and coastal Portuguese systems, Application of the United States national estuarine eutrophication assessment to the Minho, Lima, Douro, Ria de Aveiro, Mondego, Tagus, Sado, Mira, Ria Formosa. Instituto da Água & Institute of Marine Research, p. 151.

Figueiredo, N., Carranca, C., Coutinho, J., Trindade, H., Pereira, J., Prazeres, A., Marques, P., 2014. Climate Change on Ammonium "Fixation" in Flooded Rice (*Oryza Sativa*) Soils. Actas do Encontro Anual da SPCS 2013, Oeiras, pp. 22–28.

Fiorentino, G., Ferrio, J.P., Bogaard, A., Araus, J.L., Riehl, S., 2015. Stable isotopes in archaeobotanical research. Veg. Hist. Archaeobotany 24, 215–227. https://doi.org/10.1007/s00334-014-0492-9.

Fletcher, W., Boski, T., Moura, D., 2007. Palynological evidence for environmental and climatic change in the lower Guadiana valley, Portugal, during the last 13000 years. Holocene 17 (4), 481–494. https://doi.org/10.1177/0959683607077027.

Fletcher, W.J., Debret, M., Sanchez Goñi, M.F., 2013. Mid-Holocene emergence of a low frequency millennial oscillation in western Mediterranean climate: implications for past dynamics of the North Atlantic atmospheric westerlies. Holocene 23, 153–166. https://doi.org/10.1177/0959683612460783.

Folk, R.L., 1954. The distinction between grain size and mineral composition in sedimentary-rock nomenclature. J. Geol. 62, 344–359. https://www.jstor.org/stable/30065016.

Fonseca, R., Canário, T., Morais, M., Barriga, F.J.A.S., 2011. Phosphorus sequestration in Fe-rich sediments from two Brazilian tropical dam reservoirs. Appl. Geochem. 26, 1607–1622. https://doi.org/10.1016/j.apgeochem.2011.04.017.

Gao, X., Yang, Y., Wang, C., 2012. Geochemistry of organic carbon and nitrogen in surface sediments of coastal Bohai Bay inferred from their ratios and stable isotopic signatures. Mar. Pollut. Bull. 64, 1148–1155.

García-Artola, A., Stephan, P., Cearreta, A., Kopp, R.E., Khan, S.N., Horton, B.P., 2018. Holocene sea-level database from the Atlantic coast of Europe. Quat. Sci. Rev. 196, 177–192. https://doi.org/10.1016/j.quascirev.2018.07.031.

Gomes, S.D., Fletcher, W.J., Rodrigues, T., Stone, A., Abrantes, F., Naughton, F., 2020. Time-transgressive Holocene maximum of temperate and Mediterranean forest development across the Iberian Peninsula reflects orbital forcing. Palaeogeogr.

Palaeoclimatol. Palaeoecol. 550, 109739. https://doi.org/10.1016/j.palaeo.2020.109739.
Gonçalves, F., Antunes, M.T., 1992. Notícia explicativa da Folha 39-D Torrão, Carta Geológica de Portugal 1:50000. Serviços Geológicos de Portugal, Lisboa.
GRID - Consultas Estudos e Projectos de Engenharia, 1989. IP1-Variante de Alcácer do Sal, Ponte sobre o rio Sado e seus viadutos de acesso. Anexo 1-Travessia da baixa aluvionar. Gráficos das sondagens e ensaios "in situ". Not published.
Henriksen, K., Kemp, W.M., 1988. Nitrification in estuarine and coastal marine sediments. In: Blackburn, T.H., Sørensen, J. (Eds.), Nitrogen Cycling in Coastal Marine Environments, SCOPE. John Wiley & Sons Lds, pp. 207–250 (Chapter 10).
Herbert, R.A., 1999. Nitrogen cycling in coastal marine ecosystems. FEMS microbiology 23, 563–590.
Hua, Q., Barbetti, M., Rakowski, A.Z., 2013. Atmospheric radiocarbon for the period 1950-2010. Radiocarbon 55, 2059–2072. https://doi.org/10.2458/azu_js_rc.v55i2.16177.
INE, 2007. Anuário Estatístico da Região do Alentejo. INE, Lisboa.
Jenkinson, D.S., Colemn, K., Harkness, D.D., 1995. The influence of fertilizer nitrogen and season on the carbon-13 abundance of wheat straw. Plant Soil 171, 365–367. https://doi.org/10.1007/BF00010293.
Khan, N.S., Vane, C.H., Horton, B.P., 2015. Stable carbon isotope and C/N geochemistry of coastal wetland sediments as a sea-level indicator. In: Shennan, I., Long, A.J., Horton, B.P. (Eds.), Handbook of Sea-Level Research, first ed. © John Wiley & Sons, Ltd, pp. 295–311.
Koziorowska, K., Kuliński, K., Pempkowiak, J., 2018. Deposition, return flux, and burial rates of nitrogen and phosphorus in the sediments of two high-Arctic fjords. Oceanologia 60 (4), 431–445. https://doi.org/10.1016/j.oceano.2018.05.001.
Kristensen, E., 1990. Characterization of biogenic organic matter by stepwise thermogravimetry (STG). Biogeochemistry 9, 135–159. https://www.jstor.org/stable/1468541.
Lamb, A.L., Wilson, G.P., Leng, M.J., 2006. A review of coastal palaeoclimate and relative sea-level reconstructions using $\delta^{13}C$ and C/N rations in organic material. Earth Sci. Rev. 75, 29–57. https://doi.org/10.1016/j.earscirev.2005.10.003.
Leorri, E., Cearreta, A., Milne, G., 2012. Field observations and modelling of Holocene sea-level changes in the southern Bay of Biscay: implication for understanding current rates of relative sea-level change and vertical land motion along the Atlantic coast of SW Europe. Quat. Sci. Rev. 42, 59–73. https://doi.org/10.1016/j.quascirev.2012.03.014.
Liu, W.-C., Chen, W.-B., Cheng, R.T., Hsu, M.-H., Kuo, A.Y., 2007. Modeling the influence of river discharge on salt intrusion and residual circulation in Danshuei River estuary, Taiwan. Continent. Shelf Res. 27, 900–921. https://doi.org/10.1016/j.csr.2006.12.005.
Marino, R.W., Howarth, R., 2009. Nitrogen fixation. In: Likens, G.E. (Ed.), Encyclopedia of Inland Waters, Inorganic Chemicals: Cycles and Dynamics. Academic Press, Elsevier Science (Verlag), pp. 65–72.
Martins, F., Leitão, P., Silva, A., Neves, R., 2000. 3D modelling in the Sado estuary using a new generic vertical discretization approach. Oceanol. Acta 24 (Suppl. ment), S51–S62.
Maselli, V., Trincardi, F., 2013. Man made deltas. Sci. Rep. 3, 1926. https://doi.org/10.1038/srep01926.
Matos, J.X., Oliveira, V., 2003. Mina do Lousal (Faixa Piritosa Ibérica) - Percurso geológico e mineiro pelas cortas e galerias da antiga mina, 2. IGME, Pub. Museo Geominero, pp. 117–128.
Meyers, P.A., 1994. Preservation of elemental and isotopic source identification of sedimentary organic matter. Chem. Geol. 144, 289–302. https://doi.org/10.1016/0009-2541(94)90059-0.
Meyers, P.A., 1997. Organic geochemical proxies of paleoceanographic, paleolimnologic, and paleoclimatic processes. Org. Chem. 27 (5–6), 213–250. https://doi.org/10.1016/S0146-6380(97)00049-1.
Moreira, M.E., 1992. Recent saltmarsh changes and sedimentation rates in the Sado estuary, Portugal. J. Coast Res. 8, 631–640.
Moreira, S., 2016. Contributo da geoquímica e sedimentologia na caracterização de influências antrópicas em ambientes estuarinos. PhD Thesis. Universidade de Lisboa, Lisboa.
Mota, R., 2017. Prospeção geofísica, pelo método da resistividade elétrica, no âmbito do projecto "Sociedades costeras en un mundo cambiante: studio diacrónico comparado de la prehsitoria del SO de Europa desde el Paleolítico final al Neolítico". I&D GEOTECNIA, Relatório 46'/2017 - DG/NGEA. Laboratório Nacional de Engenharia Civil.
Murphy, J., Riley, J.P., 1962. A modified single solution method for the determination of phosphate in natural waters. Anal. Chim. Acta 27, 31–36.
Neves, F., 2010. Dynamics and Hydrology of the Tagus Estuary: Results from in Situ Observations. Departamento de Geologia da Faculdade de Ciências, Universidade de Lisboa, Portugal. PhD thesis.
Ospino, S., Restrepo, J.C., Otero, L., Pierini, J., Alvarez-Silva, O., 2018. Saltwater intrusion into a river with high fluvial discharge: a microtidal estuary of the Magdalena River, Colobia. J. Coast Res. 34 (6), 1273–1288. https://doi.org/10.2112/JCOASTRES-D-17-00144.1.
Oueslati, O., Girolamo, A.M., Abouabdillah, A., Kjeldsen, T.R., Lo Porto, A., 2015. Classifying the flow regimes of Mediterranean streams using multivariate analysis. Hydrol. Process. 29, 4666–4682. https://doi.org/10.1002/hyp.10530.
Pansu, M., Gautheyrou, J., 2006. Handbook of Soils Analysis – Mineralogical, Organic and Inorganic Methods. Springer.
Pardo, P., Rauret, G., López-Sánchez, J., 2003. Analytical approaches to the determination of phosphorus partitioning patterns in sediments. J. Environ. Monit. 5, 312–318. https://doi.org/10.1039/B210354K.
Pimentel, N.L., 2002. Pedogenic and early diagenetic processes in Palaeogene alluvial fan and lacustrine deposits from the Sado Basin (S Portugal). Sediment. Geol. 148 (1–2), 123–138.
Pimentel, N.L.V., Pimentel, P.R.V., Azevêdo, T.M., Andrade, C., Freitas, M.C., Pereira, D. I., 2001. Estudo sedimentológico e geoquímico de depósitos holocénicos do rio Sado. V REQUI/I CQPLI, Lisboa, pp. 125–127.
Pleuger, E., Goiran, J.-Ph, Mazzini, I., Delile, H., Abichou, A., Gadhoum, A., Djerbi, H., Piotrowska, N., Wilson, A., Fentress, E., Ben Jerbania, I., Fagel, N., 2019. Palaeogeographical and palaeoenvironmental reconstruction of the Medjerda delta (Tunisia) during the Holocene. Quat. Sci. Rev. 220, 263–278. https://doi.org/10.1016/j.quascirev.2019.07.017.
Psuty, N.P., Moreira, M.E., 2000. Holocene sedimentation and sea level rise in the Sado estuary, Portugal. J. Coast Res. 16 (1), 125–138.
Reimer, P., Austin, W., Bard, E., Bayliss, A., Blackwell, P., Bronk Ramsey, C., Butzin, M., Cheng, H., Edwards, R., Friedrich, M., Grootes, P., Guilderson, T., Hajdas, I., Heaton, T., Hogg, A., Hughen, K., Kromer, B., Manning, S., Muscheler, R., Palmer, J., Pearson, C., van der Plicht, J., Reimer, R., Richards, D., Scott, E., Southon, J., Turney, C., Wacker, L., Adolphi, F., Büntgen, U., Capano, M., Fahrni, S., Fogtmann-Schulz, A., Friedrich, R., Köhler, P., Kudsk, S., Miyake, F., Olsen, J., Reinig, F., Sakamoto, M., Sookdeo, A., Talamo, S., 2020. The IntCal20 Northern Hemisphere radiocarbon age calibration curve (0–55 cal kBP). Radiocarbon 62. https://doi.org/10.1017/RDC.2020.41.
Renberg, I., 1990. A procedure for preparing large sets of diatom slides from the sediment cores. J. Paleolimnol. 4, 87–90.
Robins, P.E., Lewis, M.J., Freer, J., Cooper, D.M., Skinner, C.J., Coulthard, T.J., 2018. Improving estuary models by reducing uncertainties associated with river flows. Estuar. Coast Shelf Sci. 207, 63–73. https://doi.org/10.1016/j.ecss.2018.02.015.
Rodrigues, A.M.J., 1992. Avaliação do estado ambiental de um estuário de uso múltiplo, através da análise de comunidades biosedimentares. Estuário do Sado. Department of Biological and Molecular Sciences, Universidade de Stirling, Escócia, Portugal, p. 364.
Rumolo, P., Barra, M., Gherardi, S., Marsella, E., Sprovieri, M., 2011. Stable isotopes and C/N ratios in marine sediments as a tool for discriminating anthropogenic impact. J. Environ. Monit. 13, 3399–3408. https://doi.org/10.1039/c1em10568j.
Scanes, P., Ferguson, A., Potts, J., 2017. Estuary form and function: implications for palaeoecological studies. In: Weckström, K., Saunders, K.M., Gell, P.A., Skilbeck, C. G. (Eds.), Applications of Paleoenvironmental Techniques in Estuarine Studies, Part I, Estuaries and Their Management. Springer Nature, pp. 9–44.
Schultz, D.J., Calder, J.A., 1976. Organic carbon 13C/12C variations in estuarine sediments. Geochem. Cosmochim. Acta 40, 381–385. https://doi.org/10.1016/0016-7037(76)90002-8.
Senbayram, M., Dixon, L., Gouding, K.W.T., Bol, R., 2008. Long-term influence of manure and mineral nitrogen applications on plant and soil ^{15}N and ^{13}C values from the Broadbalk Wheat Experiment. Rapid Commun. Mass Spectrom. 22, 1735–1740. https://doi.org/10.1002/rcm.3548.
Shaha, D.C., Cho, Y.-K., 2016. Salt plug formation caused by decreased river discharge in a multi-channel estuary. Nature Scientific Reports 6, 27176.
Singh, R., Bhumbl, D.K., Keefer, R.F., 2011. Recommended soil sulfate-S tests. In: The Northeast Coordinating Committee for Soil Testing, (NECC-1312), third ed., pp. 55–62 Recommended Soil Testing Procedures for the Northeastern United States, Northeastern Regional Publication No. 493.
Slomp, C.P., 2011. 5.06 - phosphorus cycling in the estuarine and coastal zones: sources, sinks, and transformations. In: Wolanski, E., McLusky, D. (Eds.), Treatise on Estuarine and Coastal Science. Academic Press, pp. 201–229. https://doi.org/10.1016/B978-0-12-374711-2.00506-4.
Thornes, J., López-Bermúdez, F., Woodward, J., 2009. Hydrology, River regimes, and sediment yield. In: The Physical Geography of the Mediterranean, first ed. Oxford University Press, pp. 229–253.
Treasure, E.R., Church, M.J., Gröcke, D.R., 2016. The influence of manuring on stable isotopes ($\delta^{13}C$ and $\delta^{15}N$) in Celtic bean (*Vicia faba* L.): archaeolobotanical and palaeodietary implications. Archaeological and Anthropological Sciences 8, 555–562. https://doi.org/10.1007/s12520-015-0243-6.
Trigo, R.M., Pozo-Vásquez, D., Osborn, T.J., Castro-Díez, Y., Gámiz-Fortis, S., Esteban-Parra, M.J., 2004. North Atlantic Oscillation influence on precipitation, river flow and water resources in the Iberian Peninsula. Int. J. Climatol. 24, 925–944. https://doi.org/10.1002/joc.1048.
Vacchi, M., Marriner, N., Morhange, C., Spada, G., Fontana, A., Rovere, A., 2016. Multiproxy assessment of Holocene relative sea-level changes in the western Mediterranean: sea-level variability and improvements in the definition of the isostatic signal. Earth Sci. Rev. 155, 172–197. https://doi.org/10.1016/j.earscirev.2016.02.002.
van der Schriek, T., Passmore, D.G., Stevenson, A.C., Rolão, J., 2007. The palaeogeography of Mesolithic settlement-subsistence and shell midden formation in the Muge valley, Lower Tagus Basin, Portugal. Holocene 17 (3), 369–385. https://doi.org/10.1177/0959683607075839.
Vis, G.-J., Kasse, C., Vandenberghe, J., 2008. Late Pleistocene and Holocene palaeogeography of the Lower Tagus Valley (Portugal): effects of relative sea level, valley morphology and sediment supply. Quat. Sci. Rev. 27, 1682–1709. https://doi.org/10.1016/j.quascirev.2008.07.003.
Vis, G.-J., Bohncke, S.J.P., Schneider, H., Kasse, C., Coenraads-Nederveen, S., Zuurbier, K., Rozema, J., 2010. Holocene flooding history of the lower Tagus valley (Portugal). J. Quat. Sci. 25 (8), 1222–1238. https://doi.org/10.1002/jqs.1401.
Vos, P.C., de Wolf, H., 1993. Diatoms as a tool for reconstructing sedimentary environments in coastal wetlands: methodological aspects. Hydrobiologia 269/70, 285–296.

Wilson, G.P., Lamb, A.L., Leng, M.J., Gonzalez, S., Huddart, D., 2005a. δ13C and C/N as potential coastal palaeoenvironmental indicators in the Mersey Estuary, UK. Quat. Sci. Rev. 24, 2015–2029. https://doi.org/10.1016/j.quascirev.2004.11.014.

Wilson, G.P., Lamb, A.L., Leng, M.J., Gonzalez, S., Huddart, D., 2005b. Variability of organic δ13C and C/N in the Mersey Estuary, UK and its implications for sea level reconstruction studies. Estuar. Coast Shelf Sci. 64, 685–698. https://doi.org/10.1016/j.ecss.2005.04.003.

Zalasiewicz, J., Waters, C.N., do Sul, J.I., Corcoran, P.L., Barnosky, A.D., Cearreta, A., Edgeworth, M., Gałuzka, A., Jeandel, C., Leinfelder, R., NcNeill, J.R., Steffen, W., Summerhayes, C., Wagreich, M., Williams, M., Wolfe, A.P., Yonan, Y., 2016. The geological cycle of plastic and their use as a stratigraphic indicator of the Anthropocene. Anthropocene 13, 4–17. https://doi.org/10.1016/j.ancene.2016.01.002.

Zhang, H., Kovar, J., 2000. Phosphorus fractionation. In: Pierzynski, G.M. (Ed.), Methods of Phosphorus Analysis for Soils, Sediments, Residuals and Waters. Southern Cooperative Series Bulletin, 396, pp. 50–59.